Catalysis Science & Technology

PAPER

View Article Online
View Journal | View Issue

Check for updates

Cite this: *Catal. Sci. Technol.*, 2017, 7, 3876

Electrochemical study of the promoting effect of Fe on oxygen evolution at thin 'NiFe–Bi' films and the inhibiting effect of Al in borate electrolyte†

Remi Fayad, Jihan Dhainy, Hiba Ghandour and Lara Halaoui *

In this study, we investigated the electrochemical effects of Fe co-deposition in thin Ni oxo/hydroxo films in borate, termed 'NiFe–Bi', electrodeposited from a Ni : Fe ratio of 9 : 1, 6 : 4, and 4 : 6 in solution. The NiFe–Bi films were investigated as-deposited and after anodic conditioning, and compared to Ni–Bi without intentional Fe doping at $Ni(OH)_2$ loading from a submonolayer to 10 layers. Fe co-deposition enhanced the oxygen evolution reaction (OER) of as-deposited NiFe–Bi films relative to as-deposited Ni–Bi; however, anodic biasing was still required to maximize catalysis. The $Ni(OH)_2$/NiOOH redox peaks of NiFe–Bi deposited from 6 : 4 and 4 : 6 Ni : Fe were more cathodic and more reversible than Ni–Bi peaks. Anodic conditioning caused the $Ni(OH)_2$/NiOOH redox peaks of Ni–Bi and NiFe–Bi to shift anodically but without narrowing of peak separation, different from the effects of Fe co-deposition. After anodic conditioning, the turnover frequency (TOF) for OER per Ni center for Ni–Bi and NiFe–Bi was more proportional to the Ni content within the first linear Tafel region, with a promoting effect of Fe, and the films exhibited similar Tafel slopes of 37–42 mV dec^{-1}. With increasing overpotential however, the TOF increased more significantly at high Fe : Ni ratio and was not proportional to the Ni content, and the Tafel slopes varied while notably decreasing for some NiFe–Bi films. Electrochemical results can support a Ni active site at low overpotential, but point to possibly different roles of Fe at low *versus* high potential. In addition, the effect of adding Fe^{3+} and Al^{3+} to the electrolyte was studied after deposition of Ni–Bi. Adding Fe resulted in reaching almost maximum activity in a single potential scan, confirming the promoting role of Fe in Ni–Bi and providing a quick alternative to applying anodic bias for hours to increase activity, while Al in the electrolyte poisoned OER catalysis at Ni–Bi and at NiFe–Bi. In the presence of both Fe and Al ions in solution however, with their opposite effects on the OER, the $Ni(OH)_2$/NiOOH redox peaks shifted anodically with potential scanning.

Received 3rd May 2017,
Accepted 24th July 2017

DOI: 10.1039/c7cy00873b

rsc.li/catalysis

Open Access Article. Published on 15 August 2017. Downloaded on 8/7/2024 12:35:05 PM.
This article is licensed under a Creative Commons Attribution-NonCommercial 3.0 Unported Licence.

Introduction

Hydrogen produced by splitting water using sunlight on a semiconductor electrode[1–3] can offer a continuous and clean energy source to meet the global energy need and limit the reliance on fossil fuel, when other renewables such as solar and wind vary with weather and the diurnal cycle. This has long been considered as a 'holy grail' in chemistry, and research into finding efficient and stable photoelectrodes and multi-electron catalysts for solar splitting of water[1,2] has continued for four decades since it was first reported on a TiO_2 photoanode.[3]

Water splitting is comprised of two half-reactions: the hydrogen evolution reaction (HER), and the oxygen evolution reaction (OER). The OER, as $4OH^- \rightarrow O_2 + 4e + 2H_2O$ in alkaline solution or $2H_2O \rightarrow O_2 + 4H^+ + 4e$ in acidic solution, is a four-electron four-proton process producing one dioxygen from two water molecules.[1,2] It is thus kinetically sluggish and requires a catalyst. Rare metal oxides RuO_2 and IrO_2 are the most active catalysts for this reaction,[1,4] but extensive current research is directed to finding stable and efficient catalysts from non-precious first row metals. Reported catalysts include spinels such as Co_3O_4 and $NiCo_2O_4$, perovskites, and pyrochlores.[1] Ni-based oxides remain as some of the best

Department of Chemistry, American University of Beirut, Beirut, Lebanon 110236. E-mail: Lara.Halaoui@aub.edu.lb

† Electronic supplementary information (ESI) available: SEM images of as-deposited $Ni–Bi)_{1mC}$ and $Ni_{0.6}Fe_{40}–Bi)_{1mC}$, $Ni–Bi)_{10mC}$ and $Ni_{0.4}Fe_{0.6}–Bi)_{10mC}$ films, and $Ni–Bi)_{400mC}$ and $Ni_{0.6}Fe_{0.4}–Bi)_{400mC}$ as-deposited and after conditioning, and EDX spectra of Ni–Bi and NiFe–Bi films. First scan CV, an intermediate scan, and a CV after anodic conditioning for $Ni_{0.9}Fe_{0.1}O_x)_{1mC}$; multiple CV scans of $Ni–Bi)_{1mC}$ in 1 M KBi showing the gradual increase in OER activity; cyclic voltammograms of the $Ni–Bi)_{1mC}$ film as a first scan in 1 M KBi before and immediately after addition of 0.16 mM Al^{3+} (source 2: 98% Al, 0.001% Fe) then after multiple CVs were acquired showing the poisoning effect of Al; multiple CV scans of $Ni–Bi)_{1mC}$ in 1 M KBi showing the increase in OER activity followed by CVs after addition of 0.16 mM Al^{3+} to KBi from two Al sources showing the decrease in OER activity after addition of the metal cation, and similarly after addition of 0.08 mM each of Al^{3+} and Fe^{3+}. Comparison of OER activity of these ultra-thin films to those of literature reports on Ni–Bi. See DOI: 10.1039/c7cy00873b

This journal is © The Royal Society of Chemistry 2017

Open Access Article. Published on 15 August 2017. Downloaded on 8/7/2024 12:35:05 PM.
This article is licensed under a Creative Commons Attribution-NonCommercial 3.0 Unported Licence.

non-noble OER catalysts in alkaline solution, and a synergistic promoting effect has been observed for their bimetallic and trimetallic oxides with metals such as Co[4–10] and Fe.[10–15] In early studies, spinel $NiCo_2O_4$ was found to be more active than NiO and Co_2O_4,[16] and Fe impurities were found to enhance Ni-oxide activity.[17] $Ni_{0.9}Fe_{0.1}O_x$ was reported[11] to have greater activity than IrO_2 and exhibit a similar activity to the best catalyst in alkaline solution ($Ba_{0.5}Sr_{0.5}Co_{0.8}Fe_{0.2}O_{3-\delta}$).[18] Promotion of NiO_x activity by other metals, including Al with Fe, has been reported in combinatorial studies.[12,19]

The rational design of OER catalysts necessitates understanding of structure–activity relations and the role of guest metals. Because electrodes for the OER may also need to operate at high overpotential – the exchange current density for HER catalysts such as Pt and Pd is on the order of 10^{-3} A cm^{-2} while that of OER catalysts such as RuO_2 is about 10^{-5} to 10^{-6} A cm^{-2} $_{-1}$ catalyst activity and stability need to be determined at low and high current densities. This is particularly essential for OER electrodes that undergo structural changes in the cell, such as NiO_x electrodes.

The transformations of NiO_x in the electrochemical medium are summarized in the following Bode diagram:[20,21]

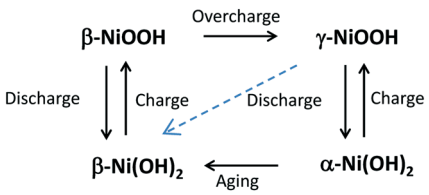

$Ni(OH)_2$ is shown to exist as one of two polymorphs, a disordered α-$Ni(OH)_2$ and a more ordered β-$Ni(OH)_2$, with a similar medium range local structure around Ni.[20,21] Associated with them are the redox couples α-$Ni(OH)_2$/γ-NiOOH and β-$Ni(OH)_2$/β-NiOOH, with a 3.6–3.8 Ni oxidation state in γ-NiOOH, and 3 in β-NiOOH.[20,21] Aging in alkaline solution or in water, or applying anodic potential, is known to transform α-$Ni(OH)_2$ into β-$Ni(OH)_2$.[21] Other transformations are β-NiOOH to γ-NiOOH by overcharging, and γ-NiOOH reduction to β-$Ni(OH)_2$. The α/γ couple has been reported to have better reversibility than β(II)/β(III), and the latter was reported to occur at more positive potential and to have greater OER activity.[20,21]

The mechanism by which Fe promotes the OER in $Ni(Fe)O_x$ remains the subject of discussions.[22–28] This has revolved around whether Ni or Fe is the active site, the role of Fe in increasing NiO_x activity, and the most active phase. Within the hypothesis of a Ni active site, Fe was proposed to exert an electronic effect on Ni;[24] Raman studies showed that Fe affects the Ni-oxide electronic environment,[14] and electronic and structural changes have been observed using Mössbauer spectroscopy.[28] Fe was also suggested to increase the conductivity of tetravalent nickel oxide or to change the mechanism.[17] It has also been proposed that Fe is the active site; a study by Bell and co-workers reported that OER intermediates adsorb too weakly on γ-NiOOH and too strongly on γ-FeOOH, while Fe sites surrounded by Ni next-nearest neighbors in γ-NiOOH had near-optimal adsorption energy.[22] Bard and co-worker reported SECM results supporting an Fe active site.[27] Stahl and co-workers suggested that an Fe^{4+} species at edges and corners could be more kinetically active for OER.[25] Regarding the most active phase, Li and Selloni determined using density functional theory that Fe-doped β-NiOOH has the lowest overpotential for OER, followed by $NiFe_2O_4$, Fe-doped γ-NiOOH, and then γ-NiOOH.[26]

High OER activity was reported by Nocera and co-workers for electrodeposited amorphous Co-[29] and Ni-[30–32](oxo)/hydroxo films in phosphate or borate (Bi) buffers, respectively, and these catalysts attracted interest after coupling to solar cells in what was termed an 'artificial leaf'.[33,34] The maximum OER activity of the Ni-based catalyst in borate, termed Ni–Bi, was reached after anodic biasing.[31] Bediako *et al.* reported that at water oxidation potentials the Ni oxidation state in 'anodized' Ni–Bi was 3.6 and resembled that in γ-NiOOH, while the oxidation state before conditioning was 3.16 and EXAFS spectroscopy showed a Jahn–Teller distorted Ni(III) phase as that in β-NiOOH.[31] The authors concluded that β-NiOOH transformed to γ-NiOOH with anodic bias and, since the OER activity increased, that γ-NiOOH is more active for OER than β-NiOOH, opposite of the views in the literature that β-NiOOH is more active.[31]

The inherent OER activity of Ni–Bi has come into question in the following work by Boettcher and co-workers that showed that the activity did not increase when the borate electrolyte was purified from Fe, and that incidental Fe doping occurs from traces of Fe.[35] This was consistent with the effect of incidental inclusion in NiO_x of Fe from KOH reported by the same group[24] and earlier by Corrigan.[17]

In this study, we investigated the electrochemical behavior of electrodeposited ultra-thin Ni–Bi films with Fe co-precipitated from Fe^{3+} and Ni^{2+} nitrates in potassium borate at Fe : Ni ratios of 1 : 9, 4 : 6, and 6 : 4. The electrochemical behavior (OER activity and redox potentials) of the films, termed NiFe–Bi, was investigated before and after anodic conditioning compared to that of Ni–Bi without intentional Fe deposition at $Ni(OH)_2$ loading from a submonolayer to 10 layers. Fe co-deposition enhanced OER activity of the as-deposited NiFe–Bi films, however anodic biasing was still needed to maximize activity. The $Ni(OH)_2$/NiOOH redox peaks of NiFe–Bi deposited from 6 : 4 and 4 : 6 Ni : Fe were more cathodic and more reversible than Ni–Bi peaks; while anodic conditioning caused the redox peaks of Ni–Bi and NiFe–Bi to shift anodically but without narrowing of peak separation, different from the effects of Fe co-deposition. After anodic conditioning, the apparent turnover frequency (TOF) for OER per Ni center at Ni–Bi and NiFe–Bi was more proportional to the Ni content within a first linear Tafel region at current densities below 1 mA cm^{-2}, with a promoting effect of Fe, and NiFe–Bi and Ni–Bi films had similar Tafel slopes of ~37–42 mV dec^{-1}. With increasing potential however, the apparent TOF per Ni center increased more significantly at high Fe : Ni ratio and was no longer proportional to the Ni content, and the Tafel slopes varied, and notably decreased for some

Open Access Article. Published on 15 August 2017. Downloaded on 8/7/2024 12:35:05 PM.
This article is licensed under a Creative Commons Attribution-NonCommercial 3.0 Unported Licence.

NiFe–Bi films. Electrochemical results can support a Ni active site at low overpotential, but point to possibly different roles of Fe at low *versus* high potential. In addition, we studied the effect of adding Fe^{3+} *versus* Al^{3+} to the electrolyte after deposition of Ni–Bi, as these two ions are known to stabilize α-$Ni(OH)_2$/γ-NiOOH, and we report that Al^{3+} in the electrolyte had a poisoning effect on the OER for Ni–Bi, and also for co-deposited NiFe–Bi, while addition of Fe^{3+} to the electrolyte resulted in reaching almost maximum activity in a single potential scan, confirming the role of Fe^{3+} in enhancing catalysis and providing a quicker alternative to applying anodic bias for hours. In the presence of both ions however, with their opposite effects on OER activity, the redox peaks shifted anodically with potential scanning.

Results and discussion

I. NiFe–Bi as-deposited films: electrochemical characterization and OER activity

I.a Electrochemical characterization of as-deposited NiFe–Bi. Ni–Bi films were electrodeposited from 0.4 mM $Ni(NO_3)_2$ in 0.1 M potassium borate (KBi) buffer pH 9.2,[31,32] at 0.953 V *vs.* Ag/AgCl at different loadings by passing charges of 0.25 mC cm^{-2}, 1 mC cm^{-2}, or 10 mC cm^{-2}. Fe-doped $Ni(OH)_2$ (NiFe–Bi) films were deposited from 0.4 mM $Ni(NO_3)_2$/$Fe(NO_3)_3$ in 0.1 M KBi at Ni : Fe ratios of 9 : 1, 6 : 4, and 4 : 6, at 1 mC cm^{-2}. Films are termed relative to the Ni : Fe ratio in the electrodeposition medium and/or the electrodeposition charge density.

Fig. 1A shows the first CV scans acquired for Ni–$Bi)_{1mC}$, Ni–$Bi)_{0.25mC}$, $Ni_{0.9}Fe_{0.1}$–$Bi)_{1mC}$, $Ni_{0.6}Fe_{0.4}$–$Bi)_{1mC}$ and $Ni_{0.4}Fe_{0.6}$–$Bi)_{1mC}$ at 10 mV s^{-1} in 1 M KBi pH 9.16. The CVs feature the well-reported quasi-reversible $Ni(OH)_2$/NiOOH redox behavior, whose redox peak potentials and peak separation depend on the phase and guest metal cation.[20,21] The $Ni(OH)_2$/NiOOH cathodic charge of Ni–$Bi)_{1mC}$ was on average 0.4 ± 0.1 mC cm^{-2}, thus only a fraction of the charge went to film deposition and the rest results from double layer charging and oxygen evolution which becomes more significant as films become thicker or with Fe included (*vide infra*). The ratio of Ni in Ni–$Bi)_{1mC}$ to Ni–$Bi)_{0.25mC}$ was 3 : 1 to 4 : 1 which is similar to the ratio of the charges; but became on average *ca.* 3.6 in Ni–$Bi)_{10mC}$ to Ni–$Bi)_{1mC}$. The peak charges and potentials depended on the %Fe in the deposition solution. Co-deposition from 40% and 60% Fe caused considerably less Ni

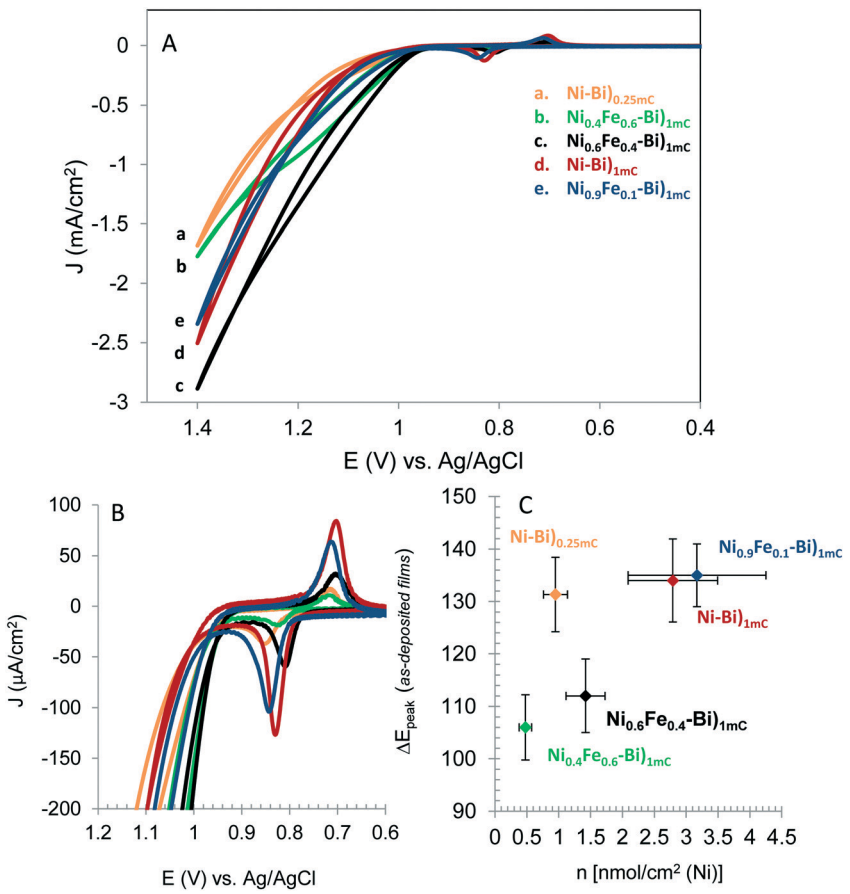

Fig. 1 (A) First cyclic voltammogram scans acquired of as-deposited films of Ni–$Bi)_{0.25mC}$ (a) $Ni_{0.4}Fe_{0.6}$–$Bi)_{1mC}$ (b), $Ni_{0.6}Fe_{0.4}$–$Bi)_{1mC}$ (c), Ni–$Bi)_{1mC}$ (d) and $Ni_{0.9}Fe_{0.1}$–$Bi)_{1mC}$ (e) at 10 mV s^{-1} in 1 M KBi pH 9.16, and (B) the same cyclic voltammograms in the potential range showing the $Ni(OH)_2$/NiOOH redox peaks. (C) ΔE_{peak} *versus* nmol cm^{-2} of Ni measured at 3 films each of Ni–$Bi)_{0.25mC}$, $Ni_{0.4}Fe_{0.6}$–$Bi)_{1mC}$, $Ni_{0.6}Fe_{0.4}$–$Bi)_{1mC}$, $Ni_{0.9}Fe_{0.1}$–$Bi)_{1mC}$, and Ni–$Bi)_{1mC}$.

 This journal is © The Royal Society of Chemistry 2017

Open Access Article. Published on 15 August 2017. Downloaded on 8/7/2024 12:35:05 PM.
This article is licensed under a Creative Commons Attribution-NonCommercial 3.0 Unported Licence.

deposition which is indicative of Fe co-precipitation since the same charge was passed, and is consistent with a report of Fe co-deposition decreasing the amount of Ni.[23] The ratio of Ni in $Ni_{0.6}Fe_{0.4}$–$Bi)_{1mC}$ to Ni–$Bi)_{1mC}$ was *ca.* 0.5 compared to the 0.6 ratio in solution, and 0.2 in $Ni_{40}Fe_{60}$–$Bi)_{1mC}$ to Ni–$Bi)_{1mC}$ compared to the 0.4 solution ratio. This is attributed to increased OER activity with more Fe co-deposited, decreasing further Ni deposition. On the other hand, 10% Fe did not reduce $Ni(OH)_2$ precipitation on average compared to Ni–$Bi)_{1mC}$ (Table 1).

Fig. 1B shows the $Ni(OH)_2$/NiOOH redox peaks of the films in Fig. 1A. Peak positions were measured at N = 3 films each. $E_{p,a}$ for Ni–$Bi)_{1mC}$ occurred at 0.836 ± 0.008 V and $E_{p,c}$ at 0.702 ± 0.000 V. The anodic peak was shifted cathodically and the cathodic peak generally was shifted anodically (5 out of 6 films, and 1 film with no change in $E_{p,c}$) for $Ni_{0.6}Fe_{0.4}$–Bi and $Ni_{0.4}Fe_{0.6}$–Bi relative to Ni–$Bi)_{1mC}$. Their respective half-wave potential $E_{1/2}$ equaled 0.764 ± 0.009 V and 0.772 ± 0.004 V, therefore there was no measurable shift from $E_{1/2}$ of Ni–$Bi)_{1mC}$ (0.769 ± 0.004 V) and $Ni_{0.9}Fe_{0.1}$–Bi (0.772 ± 0.009 V). A plot of ΔE_{peak} *versus* nmol cm^{-2} of Ni is presented in Fig. 1C, and shows narrowing in peak separation for 40% and 60% Fe in the deposition medium (N = 3 each). ΔE_p equaled 112 ± 7 mV for $Ni_{0.6}Fe_{0.4}$–Bi and 106 ± 6 mV for $Ni_{0.4}Fe_{0.6}$–Bi compared to 134 ± 8 mV for Ni–$Bi)_{1mC}$ and 135 ± 6 mV for $Ni_{0.9}Fe_{0.1}$–Bi. The increase in reversibility was not caused by lower Ni content (or in thinner films) as ΔE_p equaled 131 ± 7 mV for Ni–$Bi)_{0.25mC}$ that has Ni coverage intermediate between $Ni_{0.6}Fe_{0.4}$–Bi and $Ni_{0.4}Fe_{0.6}$–Bi. A decrease in peak separation from 101 mV to 80 mV[17] or from 150 mV to 125 mV[36] was reported by Corrigan with Fe inclusion in NiO_x, which also occurred with other ions,[36] and is another indication of Fe incorporation in $Ni_{0.6}Fe_{0.4}$–Bi and $Ni_{0.4}Fe_{0.6}$–Bi.

The inclusion of Fe therefore did not cause a thermodynamic shift in the $Ni(OH)_2$/NiOOH redox potential, but caused a kinetic facility for $Ni_{0.6}Fe_{0.4}$–Bi and $Ni_{0.4}Fe_{0.6}$–Bi. The absence of an anodic shift with Fe in NiO_x contradicts several reported observations,[17,24,25,28,35,36] from which there emerged in the literature what appears to be a consensus that Fe causes an anodic shift in the $Ni(OH)_2$/NiOOH oxidation due to an electronic effect, as discussed below.[24,25] We did not observe an anodic shift in NiFe–Bi also as we used a second source of nickel nitrate. Reviewing published work also showed that an anodic shift was not observed in every report of Fe in NiO_x.[23,27] For instance, inspection of the CVs in Fig. 1 of ref. 23 by Swierk *et al.* shows narrowing in ΔE_p and no anodic shift with Fe,[23] and the CV in Fig. 1B in the work by Scherson and co-workers does not show an anodic shift but possibly a slight cathodic shift.[37] It is not evident what causes the variability between results, but it may be due to the differences in the deposition conditions, electrolyte composition and the resulting initial film structure, since the redox peaks depend on both the phase and the guest metal cations.[20,21,36]

I.b Effect of Fe on TOF for OER in as-deposited NiFe–Bi. An apparent turnover frequency (TOF) for OER was calculated per Ni site in as-deposited NiFe–Bi from CV measurements at 10 mV s^{-1}. The Ni content was determined from the cathodic peak charge assuming 1.6 e per Ni[31] and is presented in Table 1, along with $Ni(OH)_2$ coverage and thickness assuming a film density[20,23] of 1.25 g cm^{-2} and a monolayer thickness of 8 Å.[20] The thin films were investigated to minimize the resistance and mass transport effects, and submonolayer Ni–$Bi)_{0.25mC}$ was intended to obtain a similar range of Ni contents as $Ni_{0.4}Fe_{0.6}$–$Bi)_{1mC}$ and $Ni_{0.6}Fe_{0.4}$–$Bi)_{1mC}$. It is noted that the coverage is based on $Ni(OH)_2$ content for comparison between Ni sites and does not represent the thickness of Ni–Bi films that appear to deposit as nanostructures (*vide infra*) or with Fe co-deposited. 1.6 e per Ni was assumed even though the Ni oxidation state in Ni–Bi was reported to be 3.1 before conditioning (and 3.6 in conditioned films),[31] because the cathodic charge for Ni–Bi did not change with conditioning (*cf.* Tables 1 and 2) – this could be due to scanning to positive potential overcharging to γ-NiOOH. Other researchers used 1 e per Ni.[24] The observed trend in the TOF will be the same but with lower values with 1 e per Ni.

Ni–Bi films deposited by passing a charge of 1 mC cm^{-2} thus contained on average *ca.* 2.8 nmol cm^{-2} of Ni and were *ca.* 2 nm thick (Tables 1 and 2, before and after conditioning) as calculated from the integrated cathodic peaks. The ultrathin Ni–Bi and NiFe–Bi film structure on FTO could not be discerned in the SEM images above the larger nanostructures of the FTO surface (Fig. SI.1†). The SEM images of Ni–$Bi)_{10mC}$ (Fig. SI.2†), that contained on average 10.6 nmol cm^{-2} of Ni and had a calculated thickness of *ca.* 8 nm, and of $Ni_{0.4}Fe_{0.6}$–$Bi)_{10mC}$ (Fig. SI.3†) show the films' nanoscale features grown onto the FTO nanostructures. A nanostructured film growth

Table 1 Apparent TOF for O_2 per second per Ni center calculated at different overpotentials from forward scans of the first CV acquired at 10 mV s^{-1} of as-deposited Ni–Bi and NiFe–Bi films, in unstirred 1 M KBi solution. N = 3 films, except for Ni–$Bi)_{10mC}$ where N = 2 films

Films	$nmol_{Ni}$ cm^{-2} (based on 1.6 e per Ni)	Thickness (nm)	$Monolayer_{eq}$ [$Ni(OH_2)$]	$TOF_{app,Ni,@\eta 450mV}$ (s^{-1})	$TOF_{app,Ni,@\eta 500mV}$ (s^{-1})	$TOF_{app,Ni,@\eta 650mV}$ (s^{-1})
Ni–$Bi)_{1mC}$	2.79 ± 0.70	2.07 ± 0.52	2.59 ± 0.65	0.025 ± 0.011	0.052 ± 0.023	0.676 ± 0.207
$Ni_{0.9}Fe_{0.1}$–$Bi)_{1mC}$	3.17 ± 1.08	2.35 ± 0.80	2.94 ± 1.00	0.022 ± 0.003	0.054 ± 0.027	0.813 ± 0.381
$Ni_{0.6}Fe_{0.4}$–$Bi)_{1mC}$	1.42 ± 0.31	1.05 ± 0.23	1.32 ± 0.28	0.044 ± 0.014	0.195 ± 0.090	2.156 ± 0.785
$Ni_{0.4}Fe_{0.6}$–$Bi)_{1mC}$	0.48 ± 0.10	0.35 ± 0.07	0.44 ± 0.09	0.090 ± 0.013	0.323 ± 0.072	3.698 ± 0.994
Ni–$Bi)_{250\mu C}$	0.95 ± 0.19	0.70 ± 0.14	0.88 ± 0.17	0.053 ± 0.017	0.088 ± 0.022	1.059 ± 0.344
Ni–$Bi)_{10mC}$	10.59 ± 1.47	7.85 ± 1.09	9.82 ± 1.36	0.014 ± 0.001	0.032 ± 0.010	0.617 ± 0.116

Open Access Article. Published on 15 August 2017. Downloaded on 8/7/2024 12:35:05 PM.
This article is licensed under a Creative Commons Attribution-NonCommercial 3.0 Unported Licence.

was seen in the SEM images of thicker films Ni–Bi)$_{400mC}$ and $Ni_{0.6}Fe_{0.4}$–Bi)$_{400mC}$. The SEM images of these films deposited at 400 mC cm^{-2} before and after anodization (*vide infra*) (Fig. SI.4 and SI.5†) revealed nanostructured fractal-like growth with very thin walls. Interestingly, the SEM images of $Ni_{0.6}Fe_{0.4}$–Bi)$_{400mC}$ show a difference in surface morphology with smaller nanostructures and pores compared to that of Ni–Bi)$_{400mC}$. Nocera and co-workers reported SEM images of Ni–Bi film deposited at 10 C cm^{-2} (thickness of 3 μm) and the nanostructure observed here cannot be seen in the SEM images presented for these thick films.[34] The EDX spectra revealed Ni in Ni–Bi and both Ni and Fe in NiFe–Bi films (Fig. SI.6†).

Ni–Bi)$_{1mC}$, $Ni_{0.9}Fe_{0.1}$–Bi)$_{1mC}$, $Ni_{0.6}Fe_{0.4}$–Bi)$_{1mC}$, $Ni_{0.4}Fe_{0.6}$–Bi)$_{1mC}$, and Ni–Bi)$_{0.25mC}$ in Fig. 1 contained respectively 3.02, 2.70, 1.37, 0.40 and 0.75 nmol cm^{-2} of Ni, and their equivalent thickness and $Ni(OH)_2$ coverage were: 2.24 nm and 2.8 monolayers for Ni–Bi)$_{1mC}$, 0.56 nm and 0.70 monolayer for Ni–Bi)$_{0.25mC}$, and 2.5 equivalent monolayers for $Ni_{0.9}Fe_{0.1}$–Bi, 1.3 for $Ni_{0.6}Fe_{0.4}$–Bi, and 0.37 for $Ni_{0.4}Fe_{0.6}$–Bi. Fig. 1 shows greater OER current density for $Ni_{0.6}Fe_{0.4}$–Bi)$_{1mC}$ than for Ni–Bi)$_{1mC}$ despite its two times smaller Ni content, and a greater current density for $Ni_{0.4}Fe_{0.6}$–Bi with $\theta_{Ni} \sim 0.4$ than for Ni–Bi)$_{0.25mC}$ with $\theta_{Ni} \sim 0.7$. Fig. 2 presents the currents normalized to nmol of Ni *versus* potential (E) and overpotential (η), and shows that starting from the foot of the anodic peak, currents were the largest per Ni site for $Ni_{0.4}Fe_{0.6}$–Bi, followed by $Ni_{0.6}Fe_{0.4}$–Bi, and were the lowest for Ni–Bi)$_{1mC}$ and $Ni_{0.9}Fe_{0.1}$–Bi. To determine their dependence on Fe content and thickness, the apparent TOF per electroactive Ni center at different overpotentials was calculated from the forward sweeps of the first CVs at 10 mV s^{-1} without stirring – to minimize structural changes and incidental Fe incorporation – and is presented in Table 1 and Fig. 2. At η = 450 mV at low current densities of ~13–64 μA cm^{-2} the average TOF was the highest for $Ni_{0.4}Fe_{0.6}$–Bi equaling 0.09 s^{-1}, and decreased with increasing Ni content to 0.053 s^{-1} for Ni–Bi)$_{0.25mC}$, 0.022–0.025 s^{-1} for Ni–Bi)$_{1mC}$ and $Ni_{0.9}Fe_{0.1}$–Bi, and 0.014 s^{-1} for Ni–Bi)$_{10mC}$. At η = 500 mV, at 30–159 μA cm^{-2}, the promoting effect of Fe increased, with an average TOF of 0.32 s^{-1} for $Ni_{0.4}Fe_{0.6}$–Bi and 0.20 s^{-1} for $Ni_{0.6}Fe_{0.4}$–Bi compared to 0.09 s^{-1} for Ni–Bi)$_{0.25mC}$, 0.05 s^{-1} for Ni–Bi)$_{1mC}$ and $Ni_{0.9}Fe_{0.1}$–Bi, and 0.03 s^{-1} for Ni–Bi)$_{10mC}$. At η = 650 mV, or current densities of 0.3–1.3 mA cm^{-2} for thinner films or 2.2–3.5 mA cm^{-2} for Ni–Bi)$_{10mC}$, the TOF was *ca.*

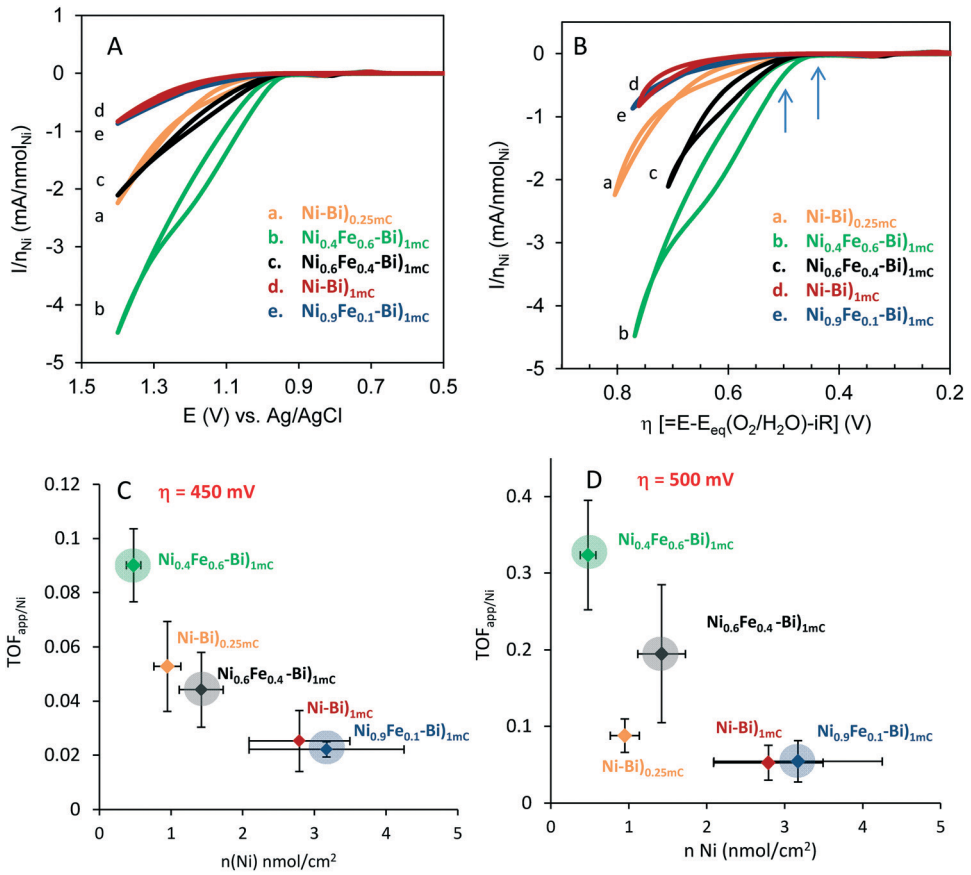

Fig. 2 Current divided per n_{Ni} *versus* potential (CVs in Fig. 1) (A) and *versus* overpotential η (B) for *as-deposited* Ni–Bi)$_{0.25mC}$ (a) $Ni_{0.4}Fe_{0.6}$–Bi)$_{1mC}$ (b), $Ni_{0.6}Fe_{0.4}$–Bi)$_{1mC}$ (c), Ni–Bi)$_{1mC}$ (d) and $Ni_{0.9}Fe_{0.1}$–Bi)$_{1mC}$ (e). Apparent turnover frequency per Ni center (TOF$_{app/Ni}$) *versus* nmol cm^{-2} of Ni measured at 3 films each of Ni–Bi)$_{0.25mC}$, $Ni_{0.4}Fe_{0.6}$–Bi)$_{1mC}$, $Ni_{0.6}Fe_{0.4}$–Bi)$_{1mC}$, $Ni_{0.9}Fe_{0.1}$–Bi)$_{1mC}$, and Ni–Bi)$_{1mC}$ at η = 450 mV (C) and η = 500 mV (D); the points for films with co-deposited Fe have shaded circles for emphasis. The arrows in panel B refer to the overpotentials for the TOF in (C) and (D).

 This journal is © The Royal Society of Chemistry 2017

Open Access Article. Published on 15 August 2017. Downloaded on 8/7/2024 12:35:05 PM.
This article is licensed under a Creative Commons Attribution-NonCommercial 3.0 Unported Licence.

3.7 s^{-1} for $Ni_{0.4}Fe_{0.6}$–Bi)$_{1mC}$, 2.2 s^{-1} for $Ni_{0.6}Fe_{0.4}$–Bi)$_{1mC}$, 1.1 s^{-1} for Ni–Bi)$_{0.25mC}$, 0.7 s^{-1} for Ni–Bi)$_{1mC}$, and 0.62 s^{-1} for Ni–Bi)$_{10mC}$.

OER activity thus decreased with increasing Ni content in as-deposited Ni–Bi and NiFe–Bi at low potential. This can indicate that only some sites – possibly at the surface – are initially catalytically active in as-deposited films even in the presence of Fe. With increasing potential, as-deposited NiFe–Bi from 60% and 40% Fe exhibited greater promotion by Fe, an effect also observed for anodically-conditioned films, and the TOF at Ni–Bi from a submonolayer to 10 layers became more proportional to the Ni content.

II. NiFe–Bi anodically-conditioned films: electrochemical characterization and OER activity

II.a Effect of anodic conditioning on NiFe–Bi films. Fig. 3 presents different scans – the first CV acquired after deposition, an intermediate CV scan as indicated, and after applying 0.903 V for ~3 h – for Ni–Bi)$_{1mC}$ (A), Ni–Bi)$_{0.25mC}$ (B), $Ni_{0.6}Fe_{0.4}$–Bi)$_{1mC}$ (C) and $Ni_{0.4}Fe_{0.6}$–Bi)$_{1mC}$ (D) in 1 M KBi at 10 mV s^{-1}. CVs for $Ni_{0.9}Fe_{0.1}$–Bi)$_{1mC}$ are presented in Fig. SI.7.† The OER activity of Ni–Bi and NiFe–Bi increased with potential scanning or applying anodic bias until maximum catalysis was reached, consistent with the reported behavior of Ni–Bi.[31] Therefore anodic conditioning was needed to form the most active catalyst even with high Fe : Ni ratio during co-deposition.

The $Ni(OH)_2$/NiOOH anodic and cathodic peaks of Ni–Bi and NiFe–Bi shifted anodically with anodic conditioning, and the reversibility of the redox couple remained unchanged. For instance, $E_{p,a}$ of Ni–Bi)$_{1mC}$ shifted to 0.871 ± 0.005 V from 0.836 ± 0.008 V and $E_{p,a}$ of $Ni_{0.6}Fe_{0.4}$–Bi)$_{1mC}$ shifted to 0.862 ± 0.016 V from 0.820 ± 0.011 V; with $E_{1/2}$ shifting by 33 ± 9 mV and 40 ± 8 mV, respectively (N = 3 each). For comparison, Bediako *et al.* reported $E_{p,a}$ of Ni–Bi in KBi at 1.05 V and ~1.025 V *vs.* NHE before and after anodic conditioning, respectively,[31] while Boettcher and co-workers reported an anodic shift that was related to Fe inclusion.[24,35] ΔE_p of anodically-conditioned $Ni_{0.6}Fe_{0.4}$–Bi and $Ni_{0.4}Fe_{0.6}$–Bi equaled 116 ± 5 mV and 106 ± 7 mV, respectively, and ΔE_p of Ni–Bi)$_{1mC}$, $Ni_{0.9}Fe_{0.1}$–Bi)$_{1mC}$, and Ni–Bi)$_{0.25mC}$ equaled 139 ± 8,

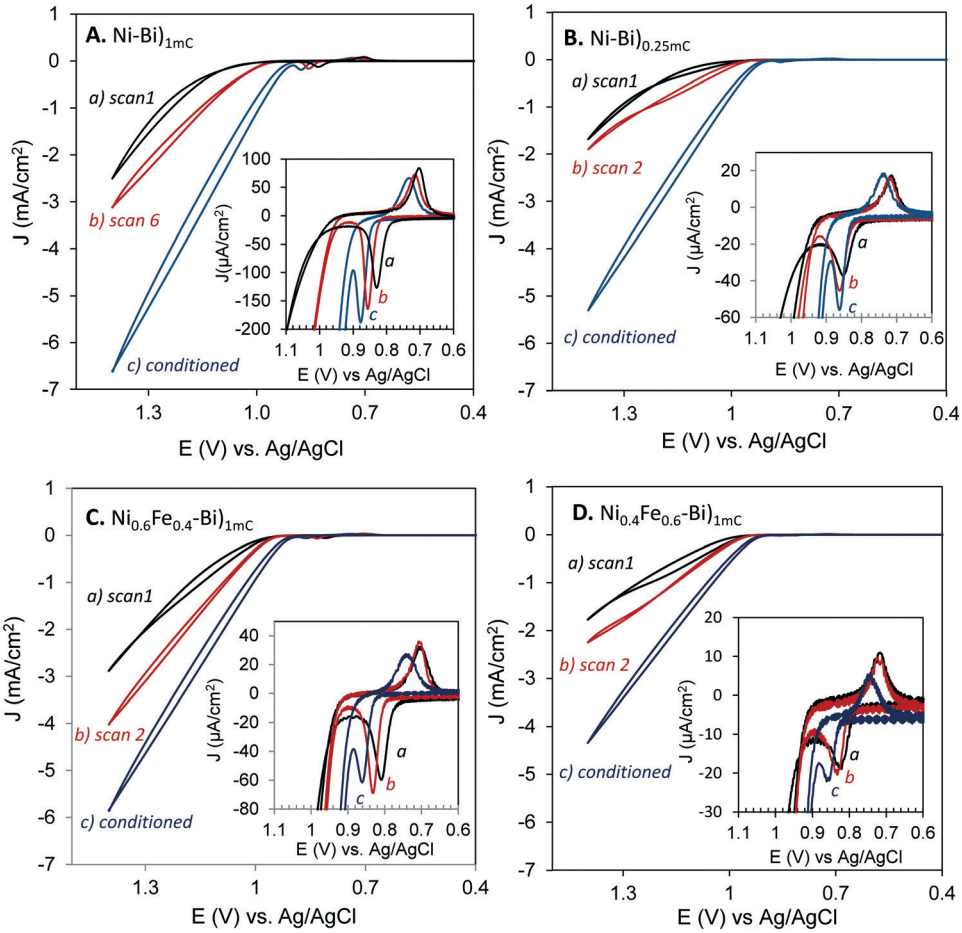

Fig. 3 First scan CV (a), an intermediate scan CV as indicated (b), and a CV after conditioning by applying an anodic bias of 0.903 V for ~3 h (c), acquired for Ni–Bi)$_{1mC}$ (A), Ni–Bi)$_{0.25mC}$ (B), $Ni_{0.6}Fe_{0.4}$–Bi)$_{1mC}$ (C) and $Ni_{0.4}Fe_{0.6}$–Bi)$_{1mC}$ (D). (The data has not been smoothed). The insets show the potential region of the $Ni(OH)_2$/NiOOH redox peaks, showing the anodic shift in the redox peaks with subsequent potential sweeps. The supporting electrolyte is 1 M KBi pH ~9.2. The scan rate is 10 mV s^{-1}.

Open Access Article. Published on 15 August 2017. Downloaded on 8/7/2024 12:35:05 PM.
This article is licensed under a Creative Commons Attribution-NonCommercial 3.0 Unported Licence.

136 ± 6, and 128 ± 6 mV, respectively, which are all similar to those before conditioning. Fe^{3+} addition to KBi that immediately increased the OER activity of Ni–Bi also did not decrease ΔE_p (*vide infra*).

Electrochemical precipitation of $Ni(OH)_2$ results in α-$Ni(OH)_2$, β-$Ni(OH)_2$, or α/β-$Ni(OH)_2$ mixed phases depending on the conditions and co-precipitation of metal cations.[21] Upon aging α-$Ni(OH)_2$ transforms into β-$Ni(OH)_2$ by loss of intercalated water and anions between sheets *via* dissolution and re-deposition or a 'zipping' mechanism.[21] Nocera and co-workers observed that as-deposited Ni–Bi is similar to β-NiOOH at water oxidation potential[31] which translates according to the Bode diagram into as-deposited reduced Ni–Bi to be similar to dehydrated β(II) (or deposited as α-$Ni(OH)_2$ that transformed to β-$Ni(OH)_2$). Co-deposition of Fe^{2+} or Fe^{3+} has been reported to lead to Fe^{3+} occupying Ni^{2+} sites in α-$Ni(OH)_2$.[38] Fe(III), Co(III) and Al(III) reportedly stabilize α-$Ni(OH)_2$ and the α/γ couple, possibly because their greater charge increases anion bonding between sheets and hinders transformation to β-$Ni(OH)_2$.[39–43] A positive shift in the $Ni(OH)_2$/NiOOH peaks and greater reversibility have been reported with Fe incorporation, and the $Ni(OH)_2$/NiOOH peaks also depend on the phase with α/γ reported to be more reversible and β(II)/β(III) to occur at more positive potentials (although some studies could have involved Fe inclusion in the electrolyte).[17,20,24,36]

Fe is thus pictured to substitute for Ni sites in Ni–Bi during co-deposition resulting in Fe-α-$Ni(OH)_2$. To explain the increase of OER activity with anodic bias at $Ni_{0.6}Fe_{0.4}$–Bi and $Ni_{0.4}Fe_{0.6}$–Bi, it could be thought that deposition from high %Fe in solution leads to segregated Fe-α-$Ni(OH)_2$, β-$Ni(OH)_2$ and $Fe(OH)_2$ regions, though the presence of one redox peak indicates that films behave as a single phase, possibly as a mixed α/β.[20,21] Dissolution and re-deposition with anodic biasing could then lead to a more uniform Fe-α-$Ni(OH)_2$/Fe-γ-NiOOH increasing activity. Dissolution and re-deposition must have led to the smoothing in the nanostructured morphology observed in the SEM images of Ni–$Bi)_{400mC}$ and $Ni_{0.6}Fe_{0.4}$–$Bi)_{400mC}$ after conditioning (Fig. SI.4 and SI.5†), which showed the same general nanostructured fractal morphology like those of as-deposited films but with smoother structures. Assuming Fe-γ-NiOOH as the active catalyst would agree with anodized Ni–Bi resembling γ-NiOOH[31] and the necessity of Fe inclusion to enhance OER at Ni–Bi.[24,35] An Fe-α-$Ni(OH)_2$/Fe-γ-NiOOH structure in anodized $Ni_{0.4}Fe_{0.6}$–Bi and $Ni_{0.6}Fe_{0.4}$–Bi agrees with the smaller peak separation reported with Fe co-precipitation and for the α/γ couple.[17,20,36] However, there would remain inconsistencies that need to be explained in this picture; the first is that the peak separation is as narrow as that in as-deposited NiFe–Bi after conditioning, and the second is that the redox couple in anodized Ni–Bi does not become more reversible as OER activity increases when Fe inclusion was reported to take place.[24,35]

The electrochemical results can be more likely explained by hypothesizing that anodic biasing causes a change in the surface-active sites while Fe is included at the surface of the films, possibly of nanocrystalline domains,[31] rather than in the internal structure. Ni–Bi was reported by Bediako *et al.* to consist of nanocrystalline oxides with the smallest ordered domains of 2–3 nm diameter.[31] Incidental Fe inclusion can occur from traces of Fe in the electrolyte, and 14% Fe inclusion has been measured by Boettcher *et al.* into NiBi (deposited at 10 mC cm^{-2}) from borate,[35] and is therefore accordingly assumed to occur as well in Ni–$Bi)_{1mC}$ – and also possibly NiFe–$Bi)_{1mC}$ – from traces in the electrolyte as reported[35] (EDX in our study cannot be used to assess the presence of Fe in Ni–Bi, note on EDX in ESI,† Fig. SI.6). It could be that Fe is modifying Ni active sites at the surface structurally or electronically or creates different active surface sites. It has been proposed for instance by Stahl and co-workers that Fe(IV) at edges and corners in NiO_x can be kinetically more active.[25] The hypothesis of surface active sites modification with including Fe explains or is not inconsistent with the following observations: 1) the presence of high %Fe in solution during co-deposition causes a smaller $Ni(OH)_2$/NiOOH redox peak separation and therefore greater kinetic facility, however subjecting Ni–Bi to anodic bias in KBi did not decrease ΔE_p even though OER activity increased, and anodic conditioning was shown to incorporate Fe in the films from the electrolyte.[35] Notably, OER activity of Ni–Bi increased immediately by addition of 0.16 mM Fe^{3+} to the electrolyte (*vide infra*) but this also did not decrease ΔE_p. The greater reversibility is therefore attributed to inclusion of Fe in the bulk of the films, but this process must be different from the one increasing OER activity with anodic bias which did not narrow ΔE_p. A greater Fe to Ni ratio could be needed inside the films (*versus* the surface) for greater reversibility during deposition of NiFe–Bi from 40% or 60% Fe. 2) The presence of high %Fe in solution during electrodeposition caused a cathodic shift while anodic conditioning caused an anodic shift in the redox peaks, pointing to the presence of two different processes. 3) ΔE_p was the same for $Ni_{0.4}Fe_{0.6}$–Bi and $Ni_{0.6}Fe_{0.4}$–Bi before and after conditioning, even as the activity increased and $E_{1/2}$ positively shifted with anodic bias application. 4) The similar OER activity per Ni site for as-deposited Ni–$Bi)_{1mC}$ and Ni–$Bi)_{10mC}$ in the first CV scan with increasing bias may indicate a structural or electronic change in surface exposed sites possibly at nanocrystalline domains,[31] rather than in sites buried in the bulk; otherwise, it would be that similar inclusion of Fe occurs in the bulk of multilayers from the first scan independent of the thickness which is a less plausible picture. Therefore, it is possible that anodic conditioning causes restructuring with inclusion of Fe to form the active catalytic surface sites, but this process does not extend fully to the bulk.

II.b Promoting effect of Fe^{3+} and poisoning effect of Al^{3+} in the electrolyte. To investigate further the effect of Fe inclusion on Ni–Bi, we compared the effects of adding to the electrolyte Fe^{3+} *versus* Al^{3+} at the same concentration, as Al^{3+} has a similar size and the same change as Fe^{3+} and is similarly known to substitute for Ni^{2+} sites and to stabilize

Open Access Article. Published on 15 August 2017. Downloaded on 8/7/2024 12:35:05 PM.
This article is licensed under a Creative Commons Attribution-NonCommercial 3.0 Unported Licence.

α-Ni(OH)$_2$/γ-NiOOH.[39–43] Fig. 4 shows CVs (at 10 mV s^{-1}) of Ni–Bi)$_{1mC}$ before and then after adding 0.16 mM Al^{3+} (source 1, 99.999% Al) or 0.16 mM Fe^{3+} to 1 M KBi, and then after acquiring 10 CVs at 100 mV s^{-1} – repeated six times. The redox peaks shifted *anodically* in the presence of both ions in consecutive scans and the oxidation peak first became sharper then broadened and was closer to the oxygen evolution wave in Fe^{3+}/KBi. In addition, the cathodic peak charge decreased indicating Ni(OH)$_2$ dissolution, but more in Al^{3+}/KBi than in Fe^{3+}/KBi. In the presence of 0.16 mM Fe^{3+}, the OER activity increased almost to the maximum after one potential scan, as seen in Fig. 4A in the significant decrease in overpotential at 1 mA cm^{-2} and the large increase in current density at high potential. This is contrasted with the more gradual increase in OER activity with potential cycling in 1 M KBi without Fe^{3+} addition (Fig. SI.8†). On the other hand, addition of 0.16 mM Al^{3+} prevented the decrease in OER overpotential observed in KBi with potential scanning (in the absence of added Al), and additionally resulted in a continuous decrease in currents at increasing potential (Fig. 4B). Addition of 0.16 mM Al^{3+} from source 2 (98% Al, 0.001% Fe) to 1 M KBi resulted in a small decrease in OER overpotential and a small increase in current density at high anodic bias in the first potential scan, but this was also followed by a decrease in current density in subsequent scans (comparing that at 1.4 V for instance, Fig. SI.9†); the difference is attributed to the presence of 0.001% Fe impurities. Therefore, Al^{3+} prevented the increase in OER activity observed with potential scanning and poisoned Ni–Bi films at higher bias. To confirm the poisoning effect of Al^{3+}, adding it to the electrolyte after the Ni–Bi OER current increased with potential scanning resulted in decreasing currents at high potential (Fig. SI.10 and SI.11† using the two Al sources), with a more significant decrease with Al with the greater purity. Al^{3+} could have been co-included or competitively included instead of Fe^{3+} present as traces in borate, or partially replaced Fe^{3+} present in Ni–Bi in these two experiments.

In addition, the effect of adding 0.16 mM Al^{3+} (99.999%) to 1 M KBi on OER for co-deposited Ni$_{0.6}$Fe$_{0.4}$–Bi)$_{1mC}$ was investigated. Fig. 4C shows a first scan CV of Ni$_{0.6}$Fe$_{0.4}$–Bi)$_{1mC}$ at 10 mV s^{-1} before and after addition of Al^{3+} to 1 M KBi, then after acquiring 10 CVs at 100 mV s^{-1} – repeated six times. The first scan CV after addition of Al^{3+} showed an increase in OER activity compared to the CV in 1 M KBi – possibly indicating a restructuring of the surface. However, subsequent potential scanning resulted in a decrease in OER activity. The Ni(OH)$_2$ redox peaks also decreased in magnitude and positively shifted. There was a difference however in the behavior of Ni–Bi)$_{1mC}$ and NiFe–Bi)$_{1mC}$ that is worth noting. While in the case of Ni–Bi)$_{1mC}$, the OER activity only decreased at the high potential and the CVs are similar at the beginning of the OER wave (Fig. 4B), in the case of Ni$_{0.6}$Fe$_{0.4}$–Bi)$_{1mC}$ the currents were initially larger as expected but the subsequent decrease in the presence of Al^{3+} was observed at both low and high potential which could be caused by Al replacing Fe in NiFe–Bi, and an inherent activity that is inde-

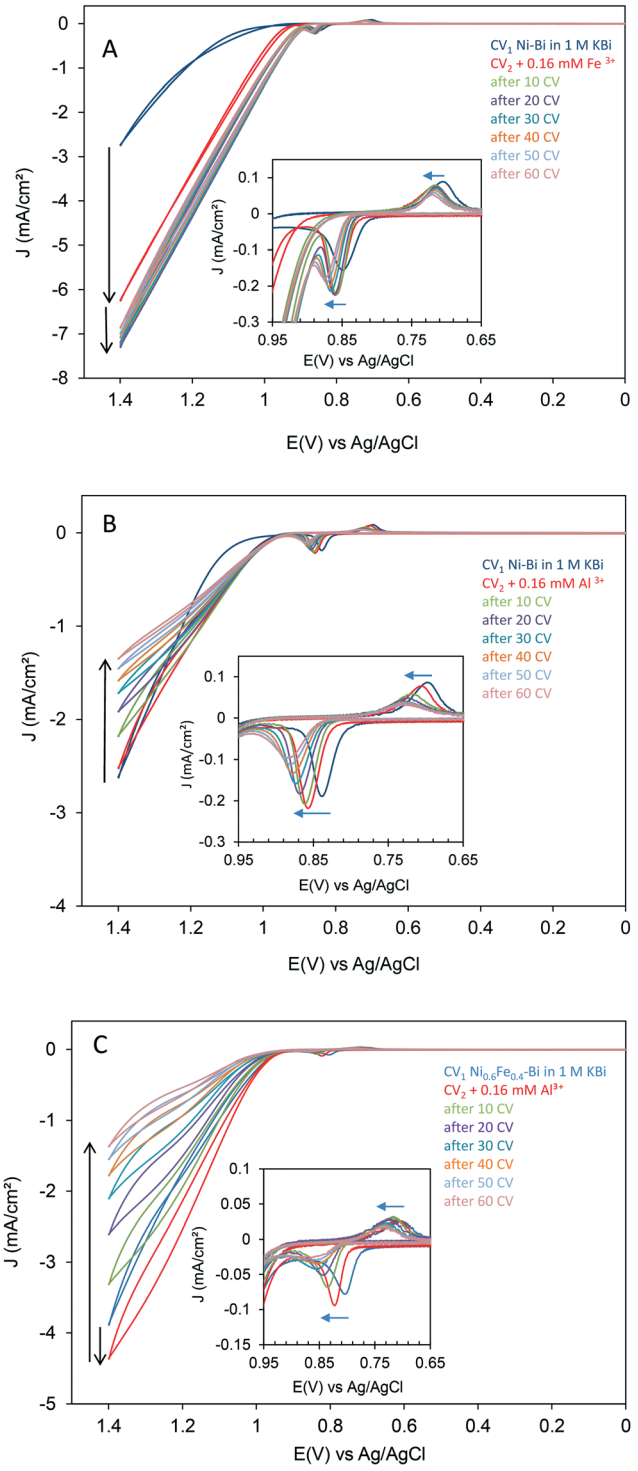

Fig. 4 Cyclic voltammograms acquired at 10 mV s^{-1} at Ni–Bi)$_{1mC}$ films as first scan in 1 M KBi before, and immediately after addition of 0.16 mM Fe^{3+} (A) or 0.16 mM Al^{3+} (B), and at Ni$_{0.6}$Fe$_{0.4}$–Bi)$_{1mC}$ film as first scan in 1 M KBi before, and immediately after addition of 0.16 mM Al^{3+} (C), then CVs acquired at 10 mV s^{-1} after 10 CVs were acquired at 100 mV s^{-1} repeated 6 times in the same solution. The number (10–60) of CVs refers to the total number of CVs at 100 mV s^{-1} that were acquired before each CV at 10 mV s^{-1}. The insets show the anodic shifts in the Ni(OH)$_2$/NiOOH peaks and decreases in charge in consecutive scans for Ni–Bi)$_{1mC}$ in the presence of 0.16 mM Fe^{3+} (inset of A) or 0.16 mM Al^{3+} (inset of B), and for NiFe–Bi)$_{1mC}$ in the presence of 0.16 mM Al^{3+} (inset of C).

Open Access Article. Published on 15 August 2017. Downloaded on 8/7/2024 12:35:05 PM.
This article is licensed under a Creative Commons Attribution-NonCommercial 3.0 Unported Licence.

pendent of Al inclusion in Ni–Bi at low potential and these differences require further study. We also investigated the competition between Al^{3+} and Fe^{3+} for co-inclusion in the films in an experiment where equal amounts of Fe^{3+} and Al^{3+} (0.08 mM each) were added to the electrolyte after deposition of Ni–Bi)$_{1mC}$ (Fig. SI.12†). The first CV in the presence of both ions showed a significant increase in OER activity resembling the immediate increase that was observed (Fig. 4A) when adding 0.16 mM Fe^{3+} albeit with smaller OER currents. However, OER currents decreased with subsequent scanning, attributed to the poisoning effect of Al^{3+} at high potential which must be co-included or competitively included in the the presence of a similar amount of Fe^{3+} in solution.

The poisoning effect of Al could be attributed to reducing the number of active sites if Fe is assumed as the active site, or to inhibiting promotion by Fe, and was observed for Ni–Bi)$_{1mC}$ or when Fe is co-deposited in NiFe–Bi or when Al and Fe are present in equal amounts in the electrolyte. In the initial experiments, a similar poisoning effect was not observed when Al was added to the electrodeposition medium of Ni–Bi at a ratio of Ni : Al of 6 : 4, and the effect of Al co-inclusion in Ni–Bi films is under current study. The role of the guest metal may depend on pre-catalyst preparation and structure, as $AlNiO_x$ was reported to be as active as $FeNiO_x$,[19] and $AlFeNiO_4$ was reported to have the greatest activity amongst several bimetallic and trimetallic oxides.[12,19] (Another example is inclusion of Co that was reported to not increase OER activity of Ni-oxide by blocking its structural transformation to the active catalyst,[11] while a synergistic effect of Co in NiO_x has been observed[16]).

The promoting effect of Fe on OER activity of NiFe-oxide has been linked to a partial charge transfer effect, and this was reasoned to reconcile with the anodic shift in the redox peaks attributed to inclusion of Fe.[35,25] It is noted and requires further investigation that an anodic shift in the $Ni(OH)_2$/NiOOH redox peaks was observed with potential scanning in the presence of both ions, but was uncorrelated in this case with their opposite effects on OER activity: adding Fe^{3+} to the electrolyte caused a fast increase in OER activity with potential scanning, while adding Al^{3+} poisoned OER catalysis.

II.c Effect of Fe on OER in NiFe–Bi at low and high current density

Tafel slopes at low and high current density. Fig. 5A and B present Tafel plots (η *versus* log$J$) of Ni–Bi)$_{1mC}$ and Ni–Bi)$_{0.25mC}$ (A), and of $Ni_{0.4}Fe_{0.6}$–Bi)$_{1mC}$ and $Ni_{0.9}Fe_{0.1}$–Bi)$_{1mC}$ (B) films (for films with CVs in Fig. 1 after conditioning); and Fig. 5C presents Tafel plots of three $Ni_{0.6}Fe_{0.4}$–Bi)$_{1mC}$ films. Two linear Tafel regions were identified, the first at current densities lower than ~1 mA cm^{-2} and the second at current densities of ~1–3 mA cm^{-2}. The Tafel slopes of anodically-conditioned Ni–Bi and NiFe–Bi (N = 3 each) are presented Table 3. The slope in the first region was not dependent on %Fe during deposition, and equaled 37 ± 2 mV dec^{-1} for Ni–Bi)$_{1mC}$ and $Ni_{0.9}Fe_{0.1}$–Bi, 37 ± 1 mV dec^{-1} for $Ni_{0.6}Fe_{0.4}$–Bi, 38 ± 3 mV dec^{-1} for Ni–Bi)$_{10mC}$, 42 ± 2 mV dec^{-1} for $Ni_{0.6}Fe_{0.4}$–Bi

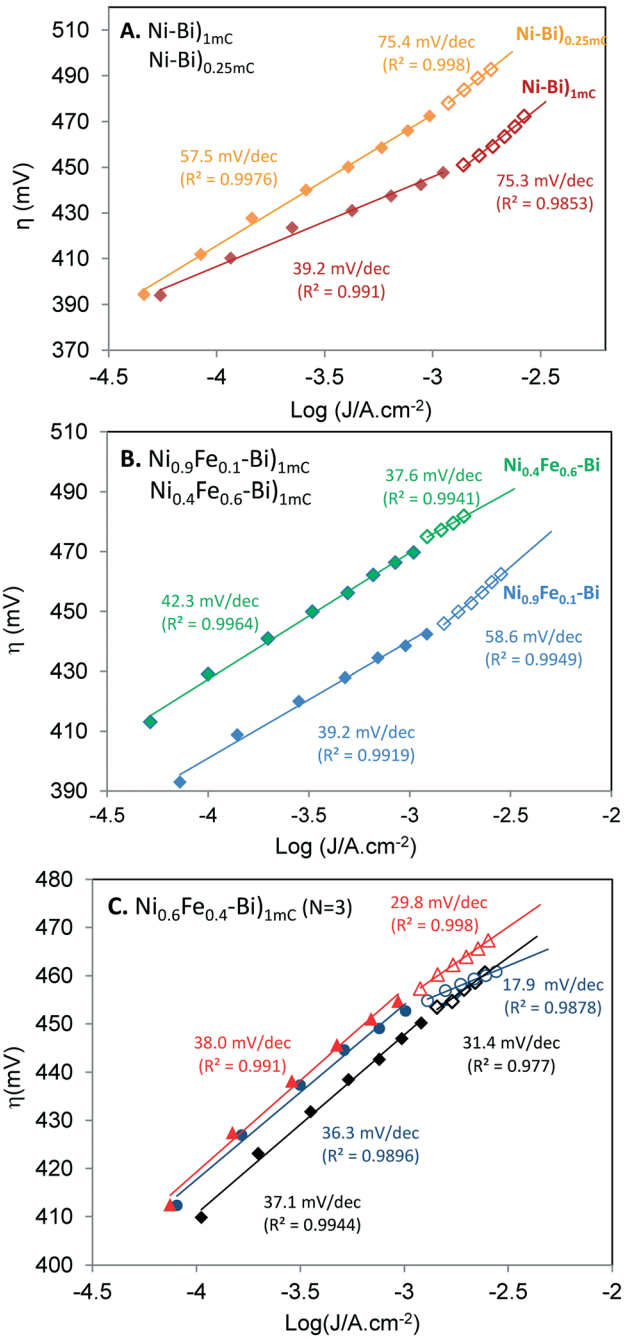

Fig. 5 Tafel plots for Ni–Bi)$_{1mC}$ and Ni–Bi)$_{0.25mC}$ (A) and for $Ni_{0.9}Fe_{0.1}$–Bi)$_{1mC}$ and $Ni_{0.4}Fe_{0.6}$–Bi)$_{1mC}$ (B), for films with CVs in Fig. 1 after anodic conditioning. (C) Tafel plots for 3 independently prepared $Ni_{0.6}Fe_{0.4}$–Bi)$_{1mC}$ anodically-conditioned films. The Tafel slope and the correlation coefficients for the best fit line are shown in the two linear regions.

and 51 ± 6 mV dec^{-1} for Ni–Bi)$_{0.25mC}$. The larger slope of NiBi)$_{0.25mC}$ could be due to a limited active area. On the other hand, the Tafel slopes were not reproducible in the second linear region. The Tafel slopes of Ni–Bi)$_{1mC}$ and Ni–Bi)$_{10mC}$ at current densities greater than ~1 mA cm^{-2} either increased or in some cases were unchanged or slightly decreased, which may be due to variations in Fe uptake from solution. The Tafel slopes of $Ni_{0.9}Fe_{0.1}$–Bi, Ni–Bi)$_{0.25mC}$ and of two of

This journal is © The Royal Society of Chemistry 2017

Open Access Article. Published on 15 August 2017. Downloaded on 8/7/2024 12:35:05 PM.
This article is licensed under a Creative Commons Attribution-NonCommercial 3.0 Unported Licence.

Table 2 Apparent TOF for O_2 per second per Ni center calculated at different overpotentials from steady-state current measurements under stirring for anodically-conditioned Ni–Bi and NiFe–Bi films in 1 M KBi solutions. The overpotential is presented as a range, as measurements were performed in potential increments of 20 mV in the same potential range for all films. N = 3 films, unless otherwise indicated; except for Ni–Bi$)_{10mC}$ where N = 2 films. The average overpotential η (mV) at which each steady state TOF was calculated is presented as italics in parenthesis

Films	$nmol_{Ni}$ cm^{-2}	Thickness (nm)	$Monolayer_{eq}$ $[Ni(OH_2)]$	TOF_{SS} (s^{-1}) (@η ~ 409–414 mV)	TOF_{SS} (s^{-1}) (@η ~ 430mV)	TOF_{SS} (s^{-1}) (@η ~ 450mV)	TOF_{SS} (s^{-1}) (@η ~ 460mV)
Ni–Bi$)_{1mC}$	2.77 ± 0.99	2.05 ± 0.73	2.57 ± 0.91	0.131 ± 0.031 (*409 ± 2*)	0.53 ± 0.15 (*430 ± 1*)	2.09 ± 0.82 (*450 ± 1*)	2.74 ± 1.62 (*457 ± 3*) (***N*** **= 2,**[a] 2.37 ± 1.00 nmol cm^{-2})
$Ni_{0.9}Fe_{0.1}$–Bi$)_{1mC}$	3.27 ± 1.09	2.42 ± 0.80	3.03 ± 1.01	0.147 ± 0.052 (*411 ± 3*)	0.494 ± 0.09 (*429 ± 2*)	1.97 ± 0.68 (*449 ± 2*)	2.35 ± 0.01 (*460 ± 0*) (***N*** **= 2,**[a] 2.65 ± 0.22 nmol cm^{-2})
$Ni_{0.6}Fe_{0.4}$–Bi$)_{1mC}$	1.10 ± 0.42	0.81 ± 0.31	1.02 ± 0.39	0.225 ± 0.079 (*411 ± 1*)	0.56 ± 0.26 (*429 ± 3*)	2.26 ± 0.81 (*449 ± 1*)	5.08 ± 0.73 (*460 ± 0*)
$Ni_{0.4}Fe_{0.6}$–Bi$)_{1mC}$	0.57 ± 0.070	0.42 ± 0.05	0.53 ± 0.065	0.225 ± 0.041 (*414 ± 1*)	0.493 ± 0.049 (*430 ± 1*)	1.73 ± 0.09 (*452 ± 2*)	3.22 ± 0.45 (*461 ± 1*)
Ni–Bi$)_{250\mu C}$	0.89 ± 0.092	0.66 ± 0.07	0.83 ± 0.085	0.161 ± 0.05 (*414 ± 2*)	0.231 ± 0.14 (*429 ± 1*)	0.96 ± 0.26 (*450 ± 4*)	1.48 ± 0.27 (*461 ± 2*)
Ni–Bi$)_{10mC}$	10.45 ± 0.22	7.75 ± 0.16	9.69 ± 0.20	0.162 ± 0.069 (*414 ± 1*)	0.45 ± 0.057 (*430 ± 1*)	—	—

[a] The numbers are the TOF of 2 out of the 3 films, since the highest potential at which the measurements were performed did not yield an overpotential of 460 mV for the third film; the corresponding number of moles is in parenthesis.

Table 3 Tafel slopes at anodically-conditioned Ni–Bi and NiFe–Bi in 1 M KBi

Films (N = 3 or 2)	$nmol_{Ni}$ cm^{-2}	$Monolayer_{eq}$ $[Ni(OH_2)]$	Slope α_1 (mV dec^{-1}) (up to ~1 mA cm^{-2})	Slope α_2 (mV dec^{-1}) (≳1 to 2–3 mA cm^{-2})	(one slope α mV dec^{-1})
Ni–Bi$)_{1mC}$	2.77 ± 0.99	2.57 ± 0.91	35	32	(34)
			39	75	
			38	35	(36)
			37 ± 2		
$Ni_{0.9}Fe_{0.1}$–Bi$)_{1mC}$	3.27 ± 1.09	3.03 ± 1.01	39	59	
			36	45	
			36	48	
			37 ± 2		
$Ni_{0.6}Fe_{0.4}$–Bi$)_{1mC}$	1.10 ± 0.42	1.02 ± 0.39	38	30	(34)
			37	31	(36)
			36	18	
			37 ± 1		
$Ni_{0.4}Fe_{0.6}$–Bi$)_{1mC}$	0.57 ± 0.07	0.53 ± 0.07	42	38	(43)
			40	48	(41)
			43	88	
			42 ± 2		
Ni–Bi$)_{250\mu C}$	0.89 ± 0.09	0.83 ± 0.09	57	75	
			46	92	
			50	141	
			51 ± 6		
Ni–Bi$)_{10mC}$	10.45 ± 0.22	9.69 ± 0.20	36	32	(34)
			40	60	
			38 ± 3		

three $Ni_{0.4}Fe_{0.6}$–Bi films increased at high overpotential but with different magnitudes, and the Tafel slope decreased for the third $Ni_{0.4}Fe_{0.6}$–Bi film. Three $Ni_{0.6}Fe_{0.4}$–Bi films exhibited an unusual decrease in their Tafel slope, from 38 mV dec^{-1} to 30 mV dec^{-1}, from 37 mV dec^{-1} to 31 mV dec^{-1}, and from 36 to 18 mV dec^{-1} (Table 3 and Fig. 5C). With the variation, a trend could be seen to emerge regarding the effect of Fe in preventing the increase in the Tafel slope at high current density.

Slopes between 30 and 40 mV dec^{-1} have been reported for NiO_x, and larger or smaller Tafel slopes were measured with increasing thickness or Fe content, respectively. Corrigan reported a slope of 50 mV dec^{-1} for NiO_x in KOH in the presence of 1 ppm iron and 40 mV dec^{-1} for thinner films, 25 mV dec^{-1} with 10% co-precipitated Fe, *ca.* 20 mV dec^{-1} at 50–75% Fe down to as low as 15 mV dec^{-1} at 75% Fe.[17] 30 mV dec^{-1} was measured by Nocera and co-workers for thin Ni–Bi[32] and 60 mV dec^{-1} for thicker films.[30] 46 mV dec^{-1} was reported by Boettcher and co-workers for Ni–Bi deposited at 10 mC cm^{-2}.[35] The Tafel slopes of Ni-oxides and other electrodes have been reported to increase at high current density.[11,17,44–46] For instance, the Tafel slope of NiO_x in KOH (in the absence of Fe) reported by Corrigan increased from 50 to 70 mV dec^{-1} at currents greater than 1 mA

Open Access Article. Published on 15 August 2017. Downloaded on 8/7/2024 12:35:05 PM.
This article is licensed under a Creative Commons Attribution-NonCommercial 3.0 Unported Licence.

cm^{-2},[17] and so did the Tafel slope of $NiCoO_x$.[11] Another example is Pt in alkaline solution with an increase from 46 mV dec^{-1} to 148 mV dec^{-1}.[44,45] An increase in the Tafel slope can be caused by a different rate determining step in the same pathway since different reactions have different potential dependencies, a variation of intermediate coverage which would manifest in linear regions with lower slopes at low overpotential and higher slopes at high overpotentials,[45,46] uncompensated resistance, and degradation or structural changes.[1] The similar behaviors of Ni–Bi)$_{1mC}$ and Ni–Bi)$_{10mC}$, and the increase in the slope for Ni–Bi)$_{0.25mC}$ do not support that resistance is causing the higher slope at high potential. Catalyst degradation can also be ruled out as a cause of the increased slope since measurements were conducted from high to low current.

On the other hand, a decrease in the Tafel slope has not been reported to our knowledge for NiO_x. However, Corrigan observed that 1 ppm Fe in solution prevented the increase in the Tafel slope of NiO_x in KOH at high overpotential, as seen in Fig. 4 of ref. 17. The Tafel behavior of $Ni_{0.6}Fe_{0.4}$–Bi and $Ni_{0.4}Fe_{0.6}$–Bi was different from that of Ni–Bi)$_{0.25mC}$, which exhibited a greater increase in the slope at high current density despite comparable Ni content, which could point to the role of Fe in preventing the same slope increase or causing its decrease. A decrease in the Tafel slope was reported for OER on Pt in sulfuric acid (from 117 mV dec^{-1} to 57 mV dec^{-1} at high potential) and was attributed by Schultze and Haga to 'resonance tunneling',[47] and by Conway and Liu to redox mediation involving higher oxidation states of Pt proposing these ideas as equivalents.[48]

Effect of Fe on OER rate at low versus high overpotential. The apparent turnover frequency for OER per Ni center was calculated from steady-state currents (TOF$_{ss}$) at different overpotentials for anodically-conditioned Ni–Bi and NiFe–Bi measured from high to low potential (Table 2). Fig. 6 shows TOF$_{ss}$ *versus* the number of moles of Ni (n_{Ni}) at average η = 409–414 mV (A), ~430 mV (B), and at ~450 and ~460 mV (C). The average TOF$_{ss}$ in the average range 409–414 mV equaled 0.23 s^{-1} for $Ni_{60}Fe_{40}$–Bi and $Ni_{40}Fe_{60}$–Bi, 0.13–0.16 s^{-1} for Ni–Bi)$_{1mC}$, Ni–Bi)$_{10mC}$ and $Ni_{0.9}Fe_{0.1}$–Bi)$_{1mC}$, and 0.16 s^{-1} for Ni–Bi)$_{0.25mC}$ (Table 2). The average TOF$_{ss}$ at ~430 mV equaled 0.45–0.56 s^{-1} for Ni–Bi)$_{1mC}$, Ni–Bi)$_{10mC}$ and NiFe–Bi with the higher average (0.56 s^{-1}) for $Ni_{0.6}Fe_{0.4}$–Bi, and was lower (0.2 s^{-1}) for Ni–Bi)$_{0.25mC}$. The average TOF$_{ss}$ for $Ni_{0.6}Fe_{0.4}$–Bi reached 5.08 ± 0.73 s^{-1} at η = 460 ± 0 mV (N = 3), greater than that for $Ni_{0.9}Fe_{0.1}$–Bi (2.35 ± 0.01 s^{-1} at 460 ± 0 mV, N = 2) and Ni–Bi)$_{1mC}$ (2.74 ± 1.62 s^{-1} at η = 457 mV ±3, N = 2). The ratio of the average TOF at 460 mV for $Ni_{0.6}Fe_{0.4}$–Bi (N = 3) to Ni–Bi)$_{1mC}$ (N = 2) and to $Ni_{0.9}Fe_{0.1}$–Bi (N = 2) is 1.85 and 2.16, respectively, compared to ratios of 1.06 and 1.13 at 430 mV (N = 3 each), and ratios of 1.08 and 1.15 at 450 mV (N = 3 each). The promoting effect of Fe in $Ni_{0.6}Fe_{0.4}$–Bi was therefore greater at higher overpotential. The difference was not as apparent when compared to the lowest overpotential range measured (at the beginning of the Tafel plot at ~409–414 mV), where these ratios were 1.7 and 1.5,

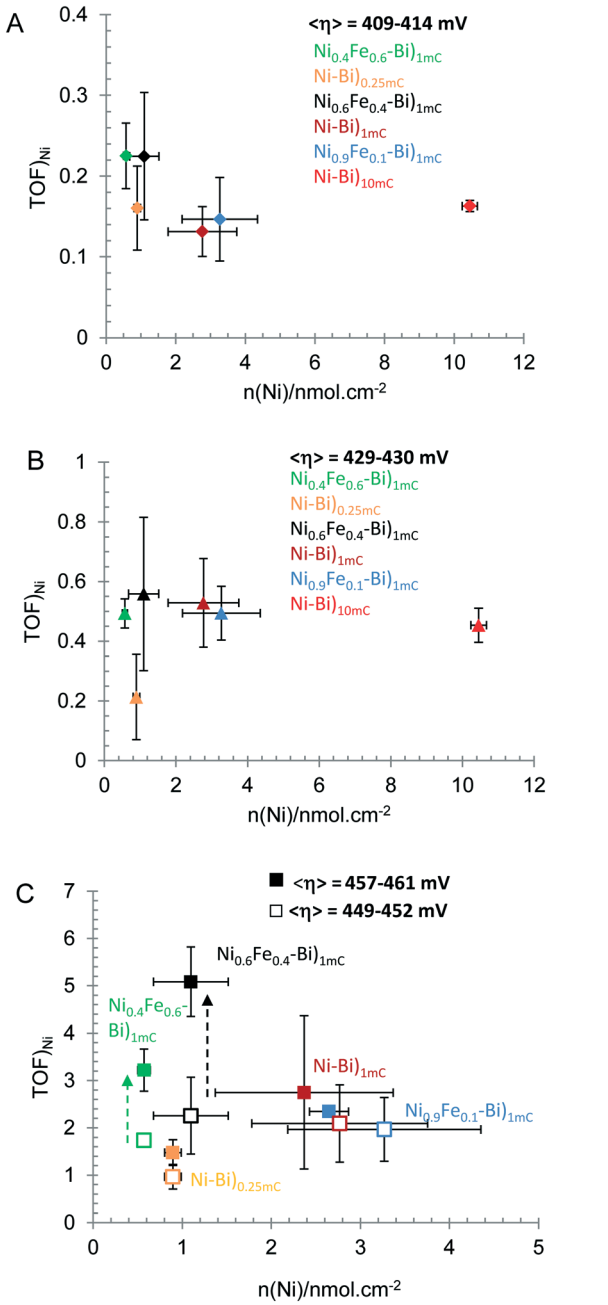

Fig. 6 Steady-state turnover frequency per Ni (TOF$_{ss}$/Ni) *versus* nmol cm^{-2} of Ni measured at anodically-conditioned Ni–Bi)$_{0.25mC}$, $Ni_{0.6}Fe_{0.4}$–Bi)$_{1mC}$, $Ni_{0.9}Fe_{0.1}$–Bi)$_{1mC}$, Ni–Bi)$_{1mC}$, and $Ni_{0.4}Fe_{0.6}$–Bi)$_{1mC}$, at average η = 409–414 mV (A); $\langle\eta\rangle$ = 429–430 mV (B); $\langle\eta\rangle$ = 449–452 mV (□) and 457–461 mV (■) (C). All measurements are for N = 3 films except for Ni–Bi)$_{1mC}$ and $Ni_{0.9}Fe_{0.1}$–Bi)$_{1mC}$ at overpotentials of 457–461 mV and for Ni–Bi)$_{10mC}$ where N = 2. Details are in Table 2.

respectively (*cf.* Table 2). At ~460 mV, the TOF of $Ni_{0.4}Fe_{0.6}$–Bi (3.22 ± 0.45 s^{-1} at 461 ± 1 mV) was 2.2-fold larger than that of Ni–Bi)$_{0.25mC}$ (1.48 ± 0.27 s^{-1} at 461 ± 2 mV) with its higher Ni content in a submonolayer coverage.

A similar general trend could also be observed from CVs at 10 mV s^{-1} without stirring but with lower TOFs. Fig. 7 shows CVs (A) and normalized current to n_{Ni} *versus* E (B) and

 This journal is © The Royal Society of Chemistry 2017

Open Access Article. Published on 15 August 2017. Downloaded on 8/7/2024 12:35:05 PM.
This article is licensed under a Creative Commons Attribution-NonCommercial 3.0 Unported Licence.

η (C) plots for anodically-conditioned Ni–Bi)$_{1mC}$, Ni$_{0.9}$Fe$_{0.1}$–Bi)$_{1mC}$, Ni$_{0.6}$Fe$_{0.4}$–Bi)$_{1mC}$ Ni$_{0.4}$Fe$_{0.6}$–Bi)$_{1mC}$ and Ni–Bi)$_{0.25mC}$. Fig. 7B shows greater normalized currents *versus* potential for Ni$_{0.4}$Fe$_{0.6}$–Bi with the smallest Ni content, followed by Ni$_{0.6}$Fe$_{0.4}$–Bi and Ni–Bi)$_{0.25mC}$. When the normalized currents are plotted *versus* overpotential in Fig. 7C promotion by Fe is seen more clearly with increasing overpotential for Ni$_{0.6}$Fe$_{0.4}$–Bi followed by Ni$_{0.4}$Fe$_{0.6}$–Bi. We note however that there was larger variability from CVs of films at higher η. At η = 420 mV, the average TOF from the CV currents was 0.142 ± 0.047 s^{-1} and 0.156 ± 0.018 for Ni–Bi)$_{1mC}$ and Ni–Bi)$_{10mC}$, respectively, and 0.27 s^{-1} ± 0.027 s^{-1} and 0.189 ± 0.020 s^{-1} for Ni$_{0.6}$Fe$_{0.4}$–Bi)$_{1mC}$ and Ni$_{0.4}$Fe$_{0.6}$–Bi)$_{1mC}$, respectively, for 3 films each. At η = 430 mV, the average TOF equaled 0.260 ± 0.073 s^{-1} for Ni–Bi)$_{1mC}$, compared to 0.403 ± 0.043 s^{-1} for Ni$_{0.6}$Fe$_{0.4}$–Bi)$_{1mC}$. At 460 and 480 mV, the average TOFs were 1.92-fold and 2.2-fold greater, respectively, of Ni$_{0.6}$Fe$_{0.4}$–Bi)$_{1mC}$ (3.065 ± 1.675 s^{-1} and 6.39 ± 3.41 s^{-1}, respectively, N = 3 each) compared to those of Ni–Bi)$_{1mC}$ (1.599 ± 0.357 s^{-1} and 2.93 ± 0.71 s^{-1}, respectively, N = 3 each), greater than the 1.55 ratio at 430 mV, but comparable on average to the 1.9 ratio at 420 mV; but with a larger variation around the mean.

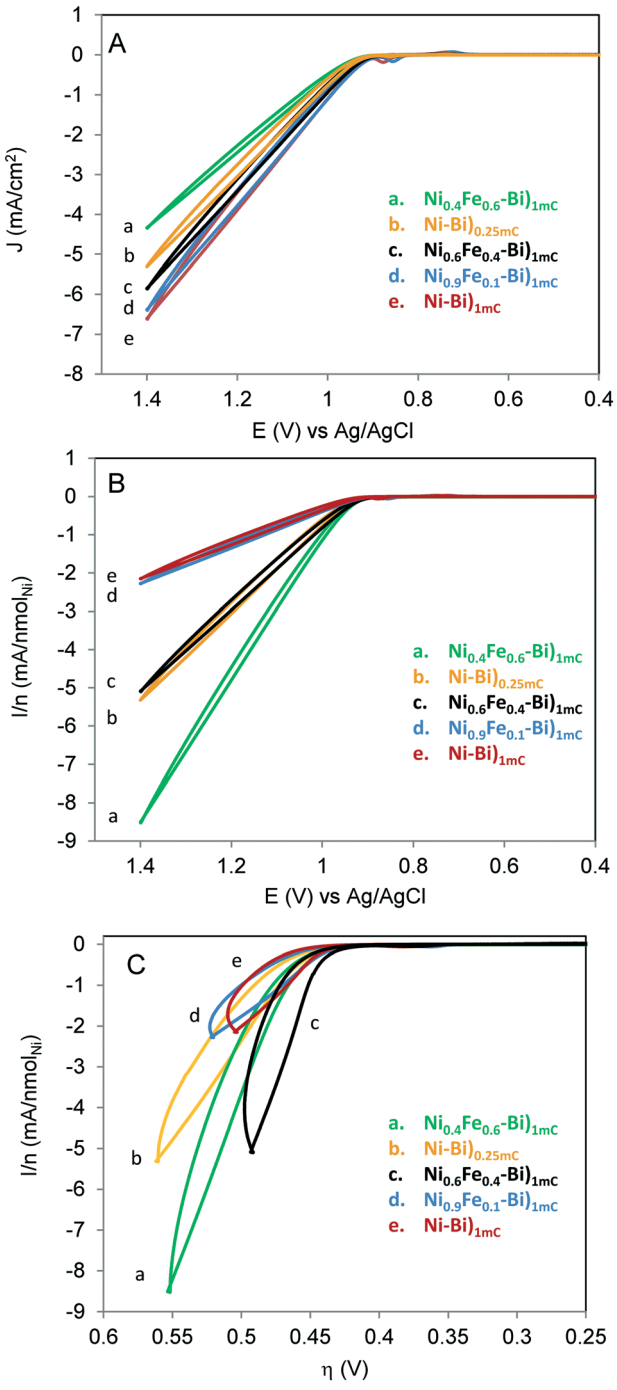

Fig. 7 Cyclic voltammograms (A), and the cyclic voltammograms plotted as current divided by nmol of Ni *vs.* potential (B) and current per nmol of Ni *vs.* overpotential η ($E - E_{eq}(O_2/H_2O) - iR$) (C) at anodically-conditioned Ni$_{0.4}$Fe$_{0.6}$–Bi)$_{1mC}$ (a), Ni–Bi)$_{0.25mC}$ (b) Ni$_{0.6}$Fe$_{0.4}$–Bi)$_{1mC}$ (c), Ni$_{0.9}$Fe$_{0.1}$–Bi)$_{1mC}$ (d), and Ni–Bi)$_{1mC}$ (e). Scan rate is 10 mV s^{-1}. Electrolyte is 1 M KBi ~pH 9.16.

A comparison of OER activity (the TOF and the overpotential needed to deliver 1 mA cm^{-2}) to reported thin Ni–Bi films[32,34,35] and nanostructured 3D Ni–Bi films[49–54] and the affecting factors are presented in detail in the ESI.† In general, the apparent steady-state TOF for the ultra-thin films in this study at low potentials is lower than that reported for Ni–Bi films, and the onset of the linear Tafel region started at higher overpotentials but shifted to lower values with increasing coverage from Ni–Bi)$_{1mC}$ to Ni–Bi)$_{10mC}$, and then to Ni–Bi)$_{100mC}$ and the overpotential needed to drive 1 mA cm^{-2} decreased with increasing coverage. A current density of 1 mA cm^{-2} was measured at steady-state at 430–440 mV for Ni–Bi)$_{1mC}$, at *ca.* 420 mV for Ni–Bi)$_{10mC}$, and at 399–404 mV for Ni–Bi)$_{100mC}$ (N = 3). By comparison, Dincă *et al.* reported 1 mA cm^{-2} at 425 mV for Ni–Bi deposited at 300 mC cm^{-2} in 1 M KBi,[34] while Bediako *et al.* reported 1 mA cm^{-2} at ~400 mV for thin Ni–Bi at 1 mC cm^{-2} (from Tafel plots presented) which contained *ca.* 5.9 nmol cm^{-2} Ni – the latter with a TOF of 0.9 s^{-1} at 400 mV[32] which is greater than that observed in this work. Boettcher *et al.* reported for Ni–Bi deposited by passing 10 mC cm^{-2} a TOF of 0.38 s^{-1} at 400 mV after conditioning, but only 0.03 s^{-1} in Fe-free electrolyte at 400 mV; meanwhile, they reported significantly greater TOFs for films with co-deposited Fe (with 1.1 e per Ni).[35] It is possible that experimental variations leading to differences in inclusion of Fe, the impurities, resistance and structure of the substrate and electrolyte concentration, could have affected the amount deposited and film coverage and therefore the catalytic activity, the onset of the Tafel region and TOF at low η. On the other hand, 3D NiBi, Ni–Co–Pi, and NiFe–Bi nanoarrays with greater catalyst loading were recently reported to yield significantly greater currents at lower overpotential, but lower TOFs and larger Tafel slopes (100–200 mV dec^{-1}).[49–54] For instance, the TOF at 600 mV for 3D Ni–Bi–Pi was 0.2 s^{-1} at 600 mV for 0.77 μmol cm^{-2} Ni,[51] and a bimetallic Ni-substituted Co–Bi on carbon cloth (3.8 μm thick) with a loading of 2.1 mg cm^{-2} that required only 388 mV to deliver 10 mA cm^{-2} was reported to have a TOF of 0.33 s^{-1} at 500 mV, and 0.2 s^{-1} at 450 mV.[49] The ultra-thin Ni–Bi)$_{1mC}$ film with ~2.8 nmol cm^{-2} yielded an apparent TOF$_{ss}$ per Ni of 2.74 ±

Open Access Article. Published on 15 August 2017. Downloaded on 8/7/2024 12:35:05 PM.
This article is licensed under a Creative Commons Attribution-NonCommercial 3.0 Unported Licence.

1.62 s^{-1} at η = 457 mV ±3 (N = 2), while the apparent TOF_{ss} at $Ni_{0.6}Fe_{0.4}$–Bi with ~1 nmol cm^{-2} Ni reached 5.08 ± 0.73 s^{-1} at η = 460 ± 0 mV (N = 3).

The mechanism by which OER activity for NiO_x is enhanced by inclusion of Fe, and whether the active site is a Ni site or an Fe site are not settled questions for NiO_x electrodes.[22–28] There are two hypotheses: one hypothesis assumes a Ni active site promoted by Fe – with possible electronic effects[14,24,28] – and the other assumes an Fe active site.[22,27] Bell and co-workers showed that Fe sites surrounded by Ni nearest neighbors in γ-NiOOH have near-optimal adsorption energy for OER intermediates.[27] The electrochemical results at low and high overpotential are discussed within these different hypotheses.

In this work, for ultra-thin Ni–Bi and NiFe–Bi films, the general proportionality of the calculated TOF per Ni center to the electrochemically accessible Ni centers at overpotentials within the first Tafel region for conditioned Ni–Bi between 2–3 layers and ~10 layers and for NiFe–Bi (at 430 mV, Fig. 6B) is a result that can be more consistent with the first hypothesis of a Ni active site with the greatest promotion by Fe at optimal doping. The effect of Fe in promoting the activity of Ni and its effect on the redox behavior of $Ni(OH)_2$ films has been discussed in the literature. Boettcher *et al.* showed that while Fe increased the conductivity of NiO_x,[24] as indicated earlier by Corrigan,[17] this did not account for the increase in OER activity.[24] They proposed that the promoting role of Fe in Ni active site occurs *via* partial charge transfer[24] – likened to the effect of the more electronegative Au support in increasing OER activity of Co-oxide by pulling electron density towards it[55,56] – and this explained the anodic shift in the $Ni(OH)_2$/NiOOH redox peak with Fe inclusion.[24] In this regard, Stahl and co-workers also presented an explanation for the anodic shift by reasoning that Fe^{3+} in the second coordination sphere will result in the oxide/hydroxide bridging ligands to have a less e-donating ability, which destabilizes Ni^{3+} and increases the redox potential.[25] Corrigan *et al.* on the other hand earlier reported *in situ* Mössbauer spectral changes that showed electronic and structural rearrangements with Fe in NiO_x, with a highly oxidized iron species as a result of partial transfer of electron densities away from Fe^{3+} sites, which could occur when the Ni^{II} sites are oxidized in Fe–$Ni(OH)_2$.[28] We observed in this work that anodic conditioning results in an anodic shift in the redox peaks, similar to the observation by Boettcher and co-workers; however Fe at 40% or 60% during co-deposition with Ni resulted in a cathodic shift in $E_{p,a}$ without a shift in $E_{1/2}$. We observed also an anodic shift in the Ni–Bi redox peaks in the presence of Al^{3+} even though OER activity was poisoned. These differences still need to be reconciled for a complete understanding of the role of Fe in the OER activity of NiO_x films, and if there is a promotion effect of a Ni site by Fe linked to the effect on the redox behavior.

On the other hand, with increasing overpotential, the apparent TOF calculated per electrochemically active Ni center was no longer on average proportional to the number of Ni centers and instead a more significant increase in TOF was measured on average for $Ni_{0.6}Fe_{0.4}$–$Bi)_{1mC}$ relative to Ni–$Bi)_{1mC}$ than at the lower potentials (Fig. 6C). In addition, the apparent TOF of ultrathin Ni–$Bi)_{0.25mC}$ which was more comparable at low overpotential (409–414 mV) to $Ni_{0.6}Fe_{0.4}$–Bi and $Ni_{0.4}Fe_{0.6}$–Bi with the comparable $Ni(OH)_2$ coverage becoming significantly lower with increasing potential. The greater increase in OER activity with Fe observed at higher overpotential for NiFe–Bi appears to be similar to the results of Corrigan for Fe-free NiO_x and NiO_x with 1 ppm Fe in KOH solution, where currents are seen to be equal at low overpotential but become higher with Fe at high overpotential.[17] These results could be pointing to a possibly different role of Fe at high overpotential, and could be consistent with a hypothesis of Fe active site with greater activity at these potentials. The effect of Al in decreasing the current of Ni–$Bi)_{1mC}$ at high potential but not at low potential can also indicate the existence of different mechanisms depending on the potential. The effect of Al in poisoning the OER activity in NiFe–Bi can support the picture of Al replacing Fe lowering activity at high potential if Fe is the active site. In this case, however, Al also poisoned OER at low potential therefore decreasing the initial promotion by Fe in as-deposited NiFe–Bi. The role of Al in Ni–Bi and NiFe–Bi and the effect of the inclusion method on the role it plays in OER are under further investigation.

Conclusions

We investigated the effect of co-precipitation of Fe with Ni in NiFe-oxo/hydroxo ultra-thin films in borate on OER catalysis and $Ni(OH)_2$/NiOOH redox behavior compared to that of Ni–Bi films with coverage from a submonolayer to multilayers. The NiFe–Bi and Ni–Bi films were investigated as-deposited and after application of anodic bias. In addition, we studied the effects of adding Fe^{3+} and Al^{3+} to the electrolyte after Ni–Bi film deposition and the effect of adding Al^{3+} after co-deposition of NiFe–Bi. The main observations and conclusions drawn from this study are summarized here: 1) as-deposited NiFe–Bi films are more active for oxygen evolution per Ni site than Ni–Bi; however they still required, similar to Ni–Bi, application of anodic bias to reach the maximum activity even with an initial Ni : Fe ratio of 40 : 60 in solution, indicating the need of a transformation to form the most active catalyst. 2) The effects of Fe co-deposition which caused more cathodic and more reversible $Ni(OH)_2$/NiOOH redox peaks were different from the effects of applying anodic bias, which caused an anodic shift and no change in peak separation of Ni–Bi and NiFe–Bi, leading to the conclusion that the process that increases OER activity with anodic bias – though it has been shown to lead to Fe inclusion – results in a different structure than when Fe is co-precipitated with Ni, consistent with the observation in (1). A possible hypothesis that can reconcile these results is that surface site modification with Fe inclusion rather than its bulk inclusion is the cause of the increase in OER activity with anodic conditioning.

 This journal is © The Royal Society of Chemistry 2017

Open Access Article. Published on 15 August 2017. Downloaded on 8/7/2024 12:35:05 PM.
This article is licensed under a Creative Commons Attribution-NonCommercial 3.0 Unported Licence.

Furthermore, we observed that addition of Fe^{3+} to the electrolyte after deposition of Ni–Bi causes a fast increase in OER activity (and therefore 3 h anodic conditioning can be replaced by this process) without narrowing the redox peaks separation, also supporting this hypothesis of surface change, while addition of Al^{3+} to the electrolyte poisoned OER catalysis for both Ni–Bi and NiFe–Bi. Noteworthy is that the redox peaks shifted anodically in the presence of both ions, with their opposite effects on catalysis. 3) The apparent TOF per Ni for OER of anodically-conditioned Ni–Bi and NiFe–Bi showed proportionality to the Ni content within the first Tafel region, which could be consistent with a Ni active site, but increased more significantly with co-deposited Fe at optimal loading at high current density. The Tafel slopes of conditioned Ni–Bi and NiFe–Bi were similar at low current density equaling 37–42 mV dec^{-1}, but variations were measured at high current density depending on the Fe content. These observations pointed to the possibility of different roles of Fe at low and high potential, which could be an Fe active site at high potential, requiring further study. Important questions thus remain with regard to the nature of the active site, and the specific structural or electronic role Fe plays in the internal or surface site catalytic activity as a function of potential and film thickness. The role of other ions such as Al^{3+} and the dependence of their effect on the mode of incorporation are also future questions for investigation. The relation between the anodic shift observed with anodic biasing and in the presence of some ions and the OER activity also requires further examination.

Experimental methods

Materials

Nickel nitrate pentahydrate ($Ni(NO_3)_2{\cdot}5H_2O$, 99.999%, trace metal analysis, Aldrich) was used for all films except for the experiments examining the effect of addition of Fe^{3+} and Al^{3+} to the potassium borate electrolyte and in the absence of added metal cations, and as the second source for testing the absence of anodic shifts with Fe co-deposition where nickel(II) nitrate hexahydrate (99.9985%, metals basis, Alfa Aesar) was used. Ferric nitrate nonahydrate ($Fe(NO_3)_3{\cdot}9H_2O$, 98%, Aldrich); aluminum nitrate nonahydrate (99.999%, trace metal basis, Acros Organics; termed source 1), aluminum nitrate nonahydrate (98% Al by EDTA titration by manufacturer, contains Fe at 0.001% by manufacturer; Baker Chemical Co.), boric acid (H_3BO_3, 99.5%, Aldrich), and potassium hydroxide (KOH, Aldrich) were used in this study. All films were electrodeposited on fluorine-doped tin oxide coated glass (FTO, R = 15 Ω sq^{-1}, except experiment in Fig. 4C R = 7 Ω sq^{-1}, Solaronix). Deionized water (resistivity 18 μΩ cm, Nanopure Diamond) was used for solution preparation.

Electrodeposition of Ni–Bi and NiFe–Bi films

FTO electrodes were cleaned by ultrasonication in isopropanol for 30 min and rinsed with water, followed by ultrasonication in water for 10–15 min, and air drying. Ni–Bi and NiFe–Bi films were electrodeposited on FTO in a 3-electrode electrochemical cell with Ag/AgCl (in saturated KCl) as the reference electrode and a 2 mm diameter Pt wire as the counter electrode. Electrodeposition was conducted from a 0.4 mM $Ni(NO_3)_3$ or 0.4 mM total concentration of $Ni(NO_3)_3$ and $Fe(NO_3)_3$ in 0.1 M KBi (aq) solution pH ~9.2 at Ni : Fe ratios of 9 : 1, 6 : 4, and 4 : 6. Films were electrodeposited by applying an anodic potential of 0.953 V *vs.* Ag/AgCl, and the amount deposited was controlled by halting the experiment when the charge reached a certain value. Ni–Bi and NiFe–Bi films were deposited by passing a charge of 1 mC cm^{-2}, while thicker Ni–Bi films were electrodeposited at 10 mC cm^{-2} and thinner films were deposited by passing a charge of 250 μC cm^{-2}. These ultra-thin $Ni(OH)_2$ films prepared by passing a charge of 250 μC cm^{-2} were intended to have a low number of Ni-sites as films obtained at 6 : 4 or 4 : 6 ratios of Ni : Fe at 1 mC cm^{-2} charge. Electrode areas were defined with insulating epoxy between 1.0 and 1.5 cm^2. Current densities are reported relative to the geometric area of the electrode.

Electrochemical measurements

Electrochemical measurements were performed in a 3-electrode electrochemical cell using a CHI Model 630A electrochemical workstation with Ag/AgCl (saturated KCl) as the reference electrode, either home-made or from Bioanalytical Systems (BAS), and a 2 mm diameter Pt wire as the counter electrode in 1 M KBi of pH ~9.2–9.4. Cyclic voltammograms were acquired by scanning the potential between −0.6 V and 1.4 V *vs.* Ag/AgCl first in the positive direction. Films were either examined as-deposited (as a first CV scan without aging) or following a procedure of anodic conditioning. Anodic conditioning consisted of holding the potential at 0.903 V *vs.* Ag/AgCl in 1 M KBi for 3 h with stirring. Cyclic voltammograms were acquired in unstirred solutions. Tafel slope measurements were performed by carrying out controlled potential electrolysis in a solution of 1 M KBi electrolyte at pH 9.2–9.4. Prior to data collection, the resistance of the solution at open circuit potential was measured using an *iR* test function to correct for ohmic potential losses. Steady-state currents were measured at different applied potentials using amperometry (*i*–*t* curves) while the solution was stirred at 600 rpm. Films required 400 to 600 s to reach a steady state. Currents were collected at potentials ranging between 1.12 V to 0.84 V *vs.* Ag/AgCl (at 20 mV increments, from high potential to low potential). Charges under the cathodic peaks were calculated using the CHI instrument's 760 software using the Gaussian peak definition. The overpotential was calculated using $\eta = E - E_{eq}(O_2/H_2O) - iR$, where $E_{eq}O_2/H_2O$ at the specific solution pH measured (in the measurements shown either 9.16 or 9.41) is calculated as follows: E_{eq} (V) = 1.23 − (0.059 × pH) + (0.059 × log(0.209)/4) − 0.197. The turnover frequency per Ni TOF was calculated as $i/4Fn_{Ni}$, where i is the current in A, F is Faraday's constant, 4

Open Access Article. Published on 15 August 2017. Downloaded on 8/7/2024 12:35:05 PM.
This article is licensed under a Creative Commons Attribution-NonCommercial 3.0 Unported Licence.

is the number of electrons per O_2 and n_{Ni} is the number of moles of Ni.

Effect of addition of Fe^{3+} and Al^{3+} to the electrolyte

Ni–Bi and $Ni_{0.6}Fe_{0.4}$–Bi films were electrodeposited on FTO at 0.953 V *vs.* Ag/AgCl by passing a charge of 1 mC cm^{-2}. Films were rinsed and moved to 20 mL of 1.0 M KBi pH ~9.2. A first CV scan was acquired at 10 mV s^{-1}, then 8 μL of either 0.4 M Fe^{3+} (for case of Ni–Bi) or 0.4 M Al^{3+} (for case of Ni–Bi or $Ni_{0.6}Fe_{0.4}$–Bi) was added to the electrolyte and mixed, or 4 μL each of Al^{3+} and Fe^{3+} in one experiment, and CV was acquired at 10 mV s^{-1} immediately after addition of the metal cations. Ten CVs were then acquired at 100 mV s^{-1}, followed by acquiring a CV at 10 mV s^{-1}. This was repeated 6 or 7 times. In one experiment, three CVs were acquired for Ni–Bi at 10 mV s^{-1}, 20 mV s^{-1} and 50 mV s^{-1} in 1 M KBi, which increased the film OER activity, before adding the 8 μL of Al^{3+}, and the experiment was continued as above.

SEM imaging and EDX

SEM images were acquired using a Tescan MIRA 3 LMU, FEG SEM, equipped with a SE detector, and an IN-Beam SE detector, and EDX spectra were acquired using an Oxford Instruments X-Max 20 EDX detector, running with Oxford INCA software.

Acknowledgements

We thank the University Research Board (URB) of the American University of Beirut for financial support of this research (Award 103186). LIH thanks Prof. D. Nocera and his group for hosting her in his laboratory at the MIT during a sabbatical in 2012, where she first became exposed and interested in Ni–Bi films. We also thank Ms. Nour Beydoun and Mr. Rida Farhat for the assistance they provided in some film preparation for SEM imaging and EDX and Mr Joan Younes (Central Research Science Laboratory, AUB) for the assistance he provided while acquiring SEM imaging and EDX analysis.

References

1 M. G. Walter, E. L. Warren, J. R. McKone, S. W. Boettcher, Q. Mi, E. A. Santori and N. S. Lewis, *Chem. Rev.*, 2010, **110**, 6446.
2 A. J. Bard, *J. Am. Chem. Soc.*, 2010, **132**, 7559.
3 A. Fujishima and K. Honda, *Nature*, 1972, **238**, 37.
4 S. Trasatti, *J. Electroanal. Chem.*, 1980, **111**, 125.
5 G. Wu, N. Li, D. R. Zhou, K. Mitsuo and B. Q. Xu, *J. Solid State Chem.*, 2004, **177**, 3682.
6 M. R. G. de Chialvo and A. C. Chialvo, *Electrochim. Acta*, 1993, **38**, 2247.
7 B. Cui, H. Lin, J. B. Li, X. Li, J. Yang and J. Tao, *Adv. Funct. Mater.*, 2008, **18**, 1440.
8 S. K. Tiwari, S. Samuel, R. N. Singh, G. Poillerat, J. F. Koenig and P. Chartier, *Int. J. Hydrogen Energy*, 1995, **20**, 9.
9 R. N. Singh, M. Hamdani, J. F. Koenig, G. Poillerat, J. L. Gautier and P. Chartier, *J. Appl. Electrochem.*, 1990, **20**, 442.
10 S. Klaus, Y. Cai, M. W. Louie, L. Trotochaud and A. T. Bell, *J. Phys. Chem. C*, 2015, **119**, 7243–7254.
11 L. Trotochaud, J. K. Ranney, K. N. Williams and S. W. Boettcher, *J. Am. Chem. Soc.*, 2012, **134**, 17253.
12 J. B. Gerken, S. E. Shaner, R. C. Masse, N. J. Porubsky and S. S. Stahl, *Energy Environ. Sci.*, 2014, **7**, 2376.
13 R. D. L. Smith, M. S. Prevot, R. D. Fagan, S. Trudel and C. P. Berlinguette, *J. Am. Chem. Soc.*, 2013, **135**, 11580.
14 M. W. Louie and A. T. Bell, *J. Am. Chem. Soc.*, 2013, **135**, 12329.
15 M. K. Bates, Q. Jia, H. Doan, W. Liang and S. Mukerjee, *ACS Catal.*, 2016, **6**, 155.
16 S. M. Jasem and A. C. C. Tseung, *J. Electrochem. Soc.*, 1979, **126**, 1353.
17 D. A. Corrigan, *J. Electrochem. Soc.*, 1987, **134**, 377.
18 J. Suntivich, K. J. May, H. A. Gasteiger, J. B. Goodenough and Y. Shao-Horn, *Science*, 2011, **334**, 1383.
19 J. Y. C. Chen, J. T. Miller, J. B. Gerken and S. S. Stahl, *Energy Environ. Sci.*, 2014, **7**, 1382.
20 M. Wehrens-Dijksma and P. H. L. Notten, *Electrochim. Acta*, 2006, **51**, 3609.
21 D. S. Hall, D. J. Lockwood, C. Bock and B. R. MacDougall, *Proc. R. Soc. A*, 2015, **471**, 20140792.
22 D. Friebel, M. W. Louie, M. Bajdich, K. E. Sanwald, Y. Cai, A. M. Wise, M. J. Cheng, D. Sokaras, T. C. Weng, R. Alonso-Mori, R. C. Davis, J. R. Bargar, J. K. Norskov, A. Nilsson and A. T. Bell, *J. Am. Chem. Soc.*, 2015, **137**, 1305.
23 J. R. Swierk, S. Klaus, L. Trotochaud, A. T. Bell and T. D. Tilley, *J. Phys. Chem. C*, 2015, **119**, 19022.
24 L. Trotochaud, S. L. Young, J. K. Ranney and S. W. Boettcher, *J. Am. Chem. Soc.*, 2014, **136**, 6744.
25 J. Y. C. Chen, L. N. Dang, H. F. Liang, W. L. Bi, J. B. Gerken, S. Jin, E. E. Alp and S. S. Stahl, *J. Am. Chem. Soc.*, 2015, **137**, 15090.
26 Y.-F. Li and A. Selloni, *ACS Catal.*, 2014, **4**, 1148.
27 H. S. Ahn and A. J. Bard, *J. Am. Chem. Soc.*, 2016, **138**, 313.
28 D. A. Corrigan, R. S. Conell, C. A. Fierro and D. A. Scherson, *J. Phys. Chem.*, 1987, **91**, 5009.
29 M. W. Kanan and D. G. Nocera, *Science*, 2008, **321**, 1072.
30 Y. Surendranath, M. W. Kanan and D. G. Nocera, *J. Am. Chem. Soc.*, 2010, **132**, 16501.
31 D. K. Bediako, B. Lassalle-Kaiser, Y. Surendranath, J. Yano, V. K. Yachandra and D. G. Nocera, *J. Am. Chem. Soc.*, 2012, **134**, 6801.
32 D. K. Bediako, Y. Surendranath and D. G. Nocera, *J. Am. Chem. Soc.*, 2013, **135**, 3662.
33 D. G. Nocera, *Acc. Chem. Res.*, 2012, **45**, 767.
34 M. Dincă, Y. Surendranath and D. G. Nocera, *Proc. Natl. Acad. Sci. U. S. A.*, 2010, **107**, 10337.
35 A. M. Smith, L. Trotochaud, M. S. Burke and S. W. Boettcher, *Chem. Commun.*, 2015, **51**, 526.
36 D. A. Corrigan and R. M. Bendert, *J. Electrochem. Soc.*, 1989, **136**, 723.

 This journal is © The Royal Society of Chemistry 2017

Open Access Article. Published on 15 August 2017. Downloaded on 8/7/2024 12:35:05 PM.
This article is licensed under a Creative Commons Attribution-NonCommercial 3.0 Unported Licence.

37 S. H. Kim, D. A. Tryk, M. R. Antonio, R. Carr and D. Scherson, *J. Phys. Chem.*, 1994, **98**, 10269.
38 M. Balasubramanian, C. A. Melendres and S. Mini, *J. Phys. Chem. B*, 2000, **104**, 4300.
39 P. Axmann and O. Glemser, *J. Alloys Compd.*, 1997, **246**, 232.
40 B. C. Cornilsen, X. Shan and P. L. Loyselle, in *Nickel Hydroxide Electrodes*, ed. D. A. Corrigan and A. H. Zimmerman, The Electrochemical Society Proceedings Series, Pennington, NJ, 1990, PV 90-4, pp. 82–96.
41 C. Delmas, J. J. Braconnier, Y. Borthomieu and P. Hagenmuller, *Mater. Res. Bull.*, 1987, **22**, 741.
42 C. Delmas, C. Faure, L. Gautier, L. GuerlouDemourgues and A. Rougier, *Philos. Trans. R. Soc., A*, 1996, **354**, 1545.
43 L. Demourguesguerlou, L. Fournes and C. Delmas, *J. Solid State Chem.*, 1995, **114**, 6.
44 B. E. Conway and T. C. Liu, *Langmuir*, 1990, **6**, 268.
45 A. Damjanovic, A. Dey and J. M. Bockris, *Electrochim. Acta*, 1966, **11**, 791–814.
46 E. Gileadi, *Electrode kinetics for chemists, chemical engineers, and materials scientists*, Capstone, 1993.
47 J. Schultze and M. Haga, *Z. Phys. Chem.*, 1977, **104**, 73.
48 B. Conway and T. Liu, *Mater. Chem. Phys.*, 1989, **22**, 163.
49 M. Ma, F. Qu, X. Ji, D. Liu, S. Hao, G. Du, A. Asiri, Y. Yao, L. Chen and X. Sun, *Small*, 2017, 1700394.
50 L. Yang, L. Xie, R. Ge, R. Kong, Z. Liu, G. Du, A. M. Asiri, Y. Yao and Y. Luo, *ACS Appl. Mater. Interfaces*, 2017, **9**, 19502.
51 M. Ma, D. Liu, S. Hao, R. Kong, G. Du, A. M. Asiri, Y. Yao and X. Sun, *Inorg. Chem. Front.*, 2017, **4**, 840.
52 L. Xie, F. Qu, Z. Liu, X. Ren, S. Hao, R. Ge, G. Du, A. M. Asiri, X. Sun and L. Chen, *J. Mater. Chem. A*, 2017, **5**, 7806.
53 R. Ge, X. Ren, F. Qu, D. Liu, M. Ma, S. Hao, G. Du, A. M. Asiri, L. Chen and X. Sun, *Chem. – Eur. J.*, 2017, **23**, 6959.
54 X. Ji, L. Ciu, D. Liu, S. Hao, J. Liu, F. Qu, Y. Ma, G. Du, A. M. Asiri and X. Sun, *Chem. Commun.*, 2017, **53**, 3070.
55 B. S. Yeo and A. T. Bell, *J. Am. Chem. Soc.*, 2011, **133**, 5587.
56 B. S. Yeo and A. T. Bell, *J. Phys. Chem. C*, 2012, **116**, 8394.